Molecular Study on the Enantiomeric Relationships of Carvedilol Fragment A, 4-(2-Hydroxypropoxy)carbazol, along with Selected Analogues

David R. P. Almeida,*,†,‡ Donna M. Gasparro,†,‡ Luca F. Pisterzi,† Ladislaus L. Torday,§ Andras Varro,§ Julius Gy. Papp,§,‖ Botond Penke,⊥ and Imre G. Csizmadia†

Department of Chemistry, Lash Miller Laboratories, 80 Saint George Street, University of Toronto, Toronto, Ontario, Canada M5S 3H6, Department of Pharmacology and Toxicology, Faculty of Medicine, Medical Sciences Building, University of Toronto, Toronto, Ontario, Canada M5S 1A8, Department of Pharmacology and Pharmacotherapy, Szeged University, Dom ter 12, Szeged, Hungary-6701, Division of Cardiovascular Pharmacology, Hungarian Academy of Sciences and Szeged University, Dom ter 12, Szeged, Hungary-6701, and Institute of Medical Chemistry, Szeged University, Dom ter 8, Szeged, Hungary-6720

Chirality and activity relationships are paramount to pharmaceutical design and synthesis. Generally, point chirality (enantiomeric *R* and *S* configurations) is emphasized most in molecules and drugs; however, axis chirality (present when structures adopt conformations with asymmetrical distributions of electron density) must also be considered as a stereogenic unit of interest. Together, stereogenic units and optical isomerism describe the chiral disposition of electron density about nuclei. In this essence, different components of chirality are always present in molecular systems. In assessing the different chiral parameters of pharmaceuticals, the cardiovascular drug carvedilol serves as an ideal example because both enantiomers produce different physiological effects. In the current study, *R*- and *S*-4-(2-hydroxypropoxy)carbazol (carvedilol fragment A), along with prochiral and chiral analogues, are studied to investigate the chiral components of carvedilol. Further, the effects of substituent variation about a stereocenter are investigated and discussed using conformational energy as a surrogate of structure (based on the fact that energy is a function of molecular spatial orientation) to determine the energetic equivalency of prochiral and chiral structures. Multidimensional conformational analysis (MDCA) was performed on selected structures using restricted Hartree−Fock (RHF) and density functional theory (DFT with the Becke 3LYP hybrid exchange-correlation functional) molecular orbital computations to elucidate the structural and energetic basis of chirality. The analogues had the following prochiral and chiral structures: R−CH$_2$−OH, [*R*] and [*S*] R−CHMe−OH, and R−CMe$_2$−OH, with substituent R being either MeCH$_2$- or ArCH$_2$-, where Ar is the carbazole moiety. Potential energy curves (PECs) of torsional angles χ_1, χ_2, χ_3, and χ_{10} for *R*- and *S*-4-(2-hydroxypropoxy)carbazol verified that all torsional angles are indeed enantiomeric. Correspondingly, the potential energy hypersurfaces (PEHSs) of *R*- and *S*-4-(2-hydroxypropoxy)carbazol were also enantiomeric, as illustrated with optimizations of conformational minima; converged minima occurred in equivalent point chiral and axis chiral pairs. Similarly to *R*- and *S*-4-(2-hydroxypropoxy)carbazol, achiral and chiral analogues analyzed by MDCA displayed axis chirality while chiral structures displayed both axis and point chirality. As such, the presence of point and axis chirality in molecular systems allows predictions to be made concerning the orientations of viable conformations of a respective PEHS. Further, the data indicate that chirality induced by an asymmetric distribution of electron density (axis chirality) is always present whenever a structure adopts asymmetric conformations. Like enantiomers of point chirality, axis chiral conformers also occur in pairs. Potential energy surfaces (PESs) were generated about the prochiral and chiral centers for all structures at the RHF/3-21G level of theory and used to test the equivalency of conformational energy between sufficiently constructed achiral and chiral structures. It is hypothesized that, with regard to conformational energy, the addition of two chiral enantiomers minus the addition of two achiral structures will give a zero result (assuming the only structural differences occur at the stereocenters). The combination of prochiral and chiral potential energy surfaces, according to an equation describing two consecutive and concerted methyl substitutions, gave a practically flat, virtually zero surface, indicating that sufficiently constructed achiral structures are energetically equivalent to chiral enantiomers. Thus, solely on the basis of molecular structure, chiral properties such as energy, number of converged conformers in a PEHS, conformations of corresponding point chiral and axis chiral pairs, and intramolecular interactions can be predicted from achiral structures. It remains to be seen how this can be utilized in drug research and development.

1. Introduction

1.1. Chirality in Pharmaceutical Agents: The Thalidomide Disaster.
Thalidomide, prescribed from 1957 to 1962 as an ex-

ceptionally safe sedative/hypnotic in adults for morning sickness, was later found to be a teratogen (capable of creating malformations in embryos). Thalidomide was blamed for having caused serious birth defects such as phocomelia (infants born without normal arms and legs) in more than 10 000 babies. Retrospective studies linked these birth defects with the mother's ingestion of thalidomide during the third to eighth week of pregnancy.

Thalidomide has one carbon stereocenter and exists as two optically active enantiomers (*R* and *S*). Tests with mice in 1961

* Corresponding author. E-mail: dalmeida@medscape.com.
† Department of Chemistry, University of Toronto.
‡ Department of Pharmacology and Toxicology, University of Toronto.
§ Department of Pharmacology and Pharmacotherapy, Szeged University.
‖ Division of Cardiovascular Pharmacology, Hungarian Academy of Sciences and Szeged University.
⊥ Institute of Medical Chemistry, Szeged University.

Enantiomeric Relationships of Carvedilol Fragment A

J. Phys. Chem. A, Vol. 107, No. 29, 2003 **5595**

suggested that only one enantiomer was teratogenic while the other possessed the desired therapeutic activity. However, subsequent tests on rabbits showed that both enantiomers had the same physiological activities. This is initially counterintuitive because one would expect enantiomers to interact quite differently with the various chiral molecules of nature. It was later verified that the enantiomers of thalidomide interconvert (racemize) under physiological conditions, causing both enantiomers to appear in the blood in roughly equal quantities.[1] Therefore, an optically or enantiomerically pure sample (containing only one enantiomer) of thalidomide versus a racemic mixture (of both enantiomers) would still produce teratogenic effects. As such, not approving thalidomide, as was done in the U.S., was the only method to prevent the thalidomide disaster.

Thalidomide is a dramatic example that chirality and activity relationships are significant to drug designers and the pharmaceutical industry, as many drug molecules synthesized exert pharmacological and physiological activities via enantiomeric-selective routes. The Food and Drug Administration (FDA) policy, published in 1992, strongly urges companies to evaluate racemates and enantiomers for new drugs for the purposes of finding the safest, most effective pharmaceuticals.[2] Methods such as computerized predictions use computational tools to predict single-enantiomer activities before separating a racemate.[3] This saves time in pharmaceutical research and helps identify the active enantiomer, leading to safer drugs. It is thus of interest to the pharmaceutical industry, and to drug research in general, to evaluate chirality exhaustively as a means to design drugs with the largest possible safety profiles.

1.2. Stereogenic Units. The importance of a point chiral stereogenic unit, as illustrated with the right-handed (R) or left-handed (S) stereocenter, is widely accepted in bio-organic chemistry. Point chiral R and S enantiomers have the same physical properties but can produce different biological and physiological effects in a molecular environment with an asymmetrical disposition (e.g., nonselective β-adrenergic receptor antagonism by $S[-]$ carvedilol). Contrasting, enantiomers may also produce the same biological effects when they interact with a symmetrical molecular environment (e.g. both enantiomers of carvedilol have equal α_1-adrenergic antagonist capabilities and antioxidant activity).

However, an asymmetric center can act not only as a stereogenic unit but also as an axis as well. Axis chirality, resulting from a clockwise [to $g+$ or plus (P)] or counterclockwise [to $g-$ or minus (M)] conformational twist, is an important phenomenon in the field of chirality. The presence of axis chirality occurs when molecular structures adopt conformations with asymmetrical electron distributions; for a given prochiral or point chiral (R and S) structure, an asymmetric molecular formation (e.g. $g+$) will have an energetically equivalent conformation with the corresponding axis chirality (e.g. $g-$). Axis chirality may play a significant role in molecular recognition or in docking at chiral active sites of enzymes or receptors. In assuming a unified viewpoint, one might say that optical isomerism provides evidence about the chiral disposition of electron density in space around the nuclei. The chirality of the electron density is always there irrespective of whether it is associated with a carbon carrying four different substituents (i.e. point chirality) or it is associated with the asymmetric electron distribution caused by a conformation twist (i.e. axis chirality).

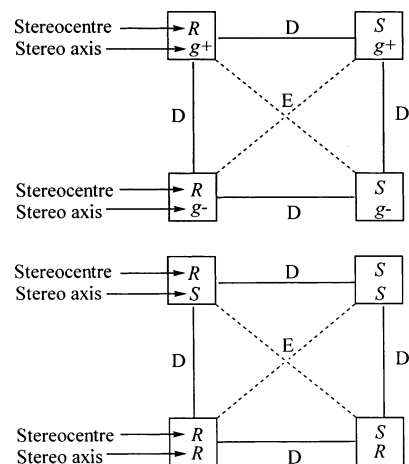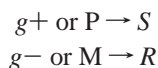In dealing with these two types of chirality, we may acknowledge the following convention for conformational twist:[4−6]

$$g+ \text{ or } P \rightarrow S$$
$$g- \text{ or } M \rightarrow R$$

Figure 1. Schematic illustration of enantiomeric (E) and diastereomeric (D) relationships for a system with one point chiral stereocenter and one stereo axis of rotation (i.e. axis chiral plane about an adjacent C−C bond) as stereogenic units.

In view of that, having one stereocenter and one rotation about an adjacent C−C bond, we may recognize four stereoisomers with enantiomeric (E) and diastereomeric (D) relationships, as shown in Figure 1.

It is then evident that, in the case of multiple rotors, the enantiomeric and diastereomeric relations are not always obvious at first sight. In the present work, we wish to report such relationships for a key fragment of the drug molecule carvedilol, 1-(9H-carbazol-4-yloxy)-3-[2-(2-methoxyphenoxy)ethylamino]-2-propanol. Fragment A of carvedilol has one stereocenter (point chiral R and S forms) and four torsional modes of motion (torsional angles) which determine the conformation of the molecular structure and the associated axis chiral parameters. Thus, fragment A has a total of five stereogenic units. It is relevant to study the characteristics of the different chiral forms of carvedilol because of its unique pharmacological profile (i.e. the two enantiomers of carvedilol possess different biological effects). The objectives of the current work are twofold: first, decompose and quantify the different chiral components of carvedilol fragment A to illustrate its full chiral profile; second, address the effects of substituent variation about a stereocenter and the basis of energetic equivalency between prochiral and chiral compounds. Conformational energy will be used as a surrogate for molecular structure because changes in structure, such as alterations in the substituents at a stereocenter, can be quantified by changes in energy. The relative effects can then be compared for given sets of compounds.

1.3. Biological and Medical Background. Carvedilol ($C_{24}H_{26}N_2O_4$) is a cardiovascular drug of proven efficacy in the treatment of mild to moderate congestive heart failure (CHF), essential hypertension, and angina and in improvement of left ventricular function. Carvedilol is a lipophilic autonomic nervous system agent that acts as a multiple-action neurohormonal antagonist by producing nonselective β-blockage (β_1 and β_2) and selective α-blockage (α_1), while also possessing myocardial-protective antioxidant properties.[7,8]

In dealing with chronic heart failure and hypertension, β-blockers block the activity of cardiac β-adrenergic receptors (both β_1 and β_2) to noradrenaline reducing the total cardiac workload of the heart.[9,10] Carvedilol provides further positive effects by vasodilation (α_1-adrenergic blockage) at peripheral resistance vessels, which decreases preload and after-load, thereby further reducing cardiac work and wall tensions.[11,12]

5596 *J. Phys. Chem. A, Vol. 107, No. 29, 2003*

Almeida et al.

The US Data and Safety Monitoring Board (US DSMB) stopped, for ethical reasons, the clinical investigation of carvedilol before its completion due to greatly lowered mortality rates.[13]

As an antioxidant, the carbazole ring of carvedilol is highly reactive with oxygen-containing radicals. Carbazole possesses a low redox potential which gives carvedilol and its metabolites a powerful tendency to donate electrons more readily in order to "scavenge" the activities of reactive oxygen species (ROS) such as oxygen superoxide ($O_2^{\bullet-}$), hydrogen peroxide (H_2O_2), hydroxyl radical ($^{\bullet}OH$), and peroxynitrite ($ONOO^-$), and as a result, it helps to protect the living body from the deleterious effects of free radical damage.[14] Carvedilol's free-radical scavenging ability against lipid peroxidation is enhanced by its relatively high lipid solubility.[15] Of interest, some of carvedilol's metabolites are more effective than carvedilol itself as antioxidants due to the fact that a hydroxyl group substitution in a heterocyclic ring, such as that of carbazole, increases the molecular antioxidant action of a compound.[13,16,17,18]

1.4. Chemical Background. Carvedilol is a chiral drug molecule (with 1 point chiral strereocenter and 11 torsional modes) commercially available as a racemic mixture of both its enantiomers ($R[+]$ and $S[-]$) (cf. Figure 2). The enantiomers of carvedilol show marked stereoselective properties in that both enantiomers have equal α_1 blocking activity and antioxidant activity but only the $S[-]$ enantiomer contains the nonselective β-adrenergic blocking activity.[16] Further, along with carvedilol, three of its hydroxylated metabolites have marked antioxidant properties while being devoid of either α_1- or β-adrenergic blocking activity (cf. Figure 2).[19,20] This represents a situation in which both enantiomers of an optically active drug offer different beneficial effects to the patient. As such, the enantiomers differ not only quantitatively in terms of potency but also qualitatively in that they possess distinct pharmacologic profiles and neither enantiomer alone has the same pharmacologic profile as the racemic mixture of carvedilol used clinically.[21]

Carvedilol was divided into three structural fragments according to its chemical activity: R- and S-4-(2-hydroxypropoxy)-carbazol (fragment A) is the antioxidant and β-blocker portion of carvedilol, 2(R and S)-1-(ethylamonium)propane-2-ol (fragment B) connects the two ether oxygens of carvedilol and possesses the protonophoretic amino group involved in the uncoupling of oxidative phosphorylation in the mitochondria,[22] and aminoethoxy-2-methoxy-benzene (fragment C) is the structure responsible for the α-blocker action of carvedilol (cf. Figure 3).

This study focuses on the chiral interactions and relationships of carvedilol by analyzing fragment A (structures **I-R** and **I-S**; cf. Figure 4), because this fragment contains the antioxidant carbazole ring system and the same point chiral stereocenter of carvedilol. Analysis was also carried out on prochiral and chiral variations of fragment A and its noncarbazole analogue. The stereocenter of fragment A is found at C24, and each of the enantiomers constitute the potential energy hypersurface (PEHS) with torsional angles χ_1, χ_2, χ_3, and χ_{10} as described by eq 1 (cf. Figure 4). The torsional angle χ_4, which is associated with the terminal methyl group, was not included because it comprises a symmetrical methyl rotation.

$$E = f(\chi_1, \chi_2, \chi_3, \chi_{10}) \tag{1}$$

The six structures—2-methoxyethan-1-ol (analogue **IV-H₂**), 1-methoxy-2-methylpropan-2-ol (analogue **IV-Me₂**), (2S)-1-methoxypropan-2-ol (analogue **III-[H,Me]-S**), (2R)-1-methoxy-propan-2-ol (analogue **III-[H,Me]-R**), (2-hydroxyethoxy)-carbazol (analogue **II-H₂**), and (2-hydroxy-2-methylethoxy)car-
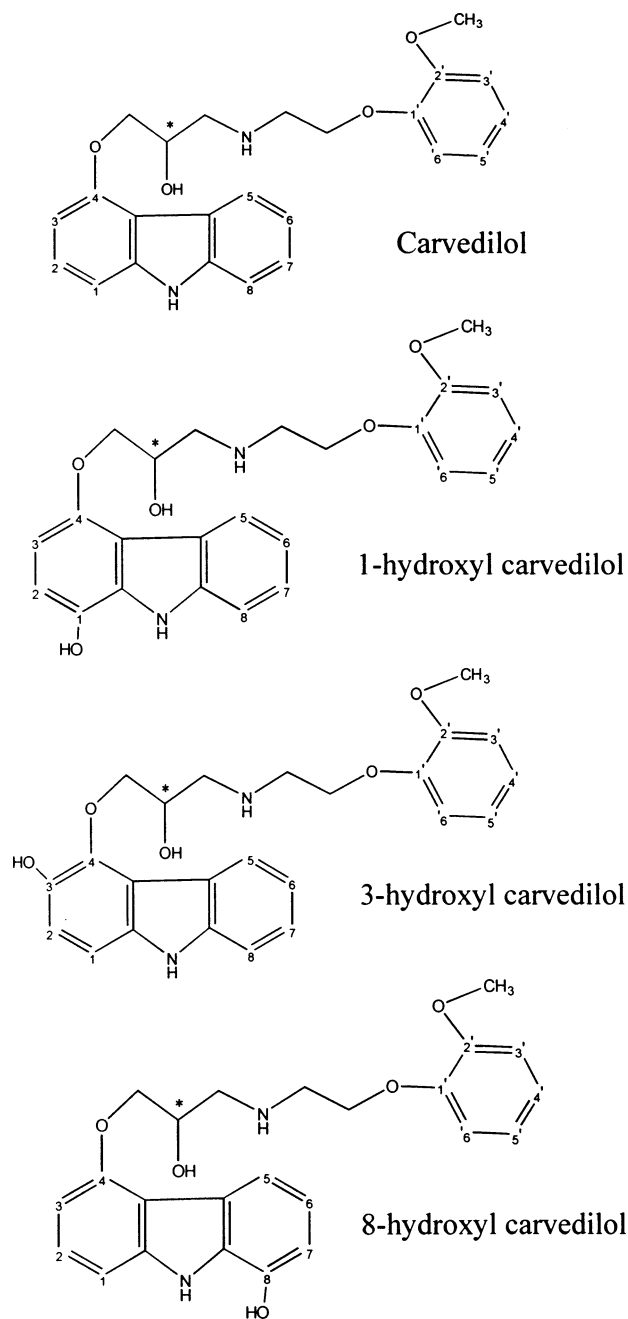
Figure 2. Structure of carvedilol and its antioxidant metabolites (IUPAC numbering used and stereocenter indicated by *).

bazol (analogue **II-Me₂**)—are presented and defined in Figure 4. The respective PEHSs of the four carbazole-containing structures can all be described by eq 1 while the remaining four structures can be described by eq 2.

$$E = f(\chi_2, \chi_3, \chi_{10}) \tag{2}$$

Structures **IV-H₂**, **IV-Me₂**, **III-[H,Me]-S**, and **III-[H,Me]-R** were constructed by replacing the bulky carbazole ring system with the simplest alkyl group, a methyl substituent. The backbone present in carvedilol, and in **I-R** and **I-S**, remained in all structures with the exceptions that **IV-H₂** was devoid of the methyl group formerly present at the chiral center while **IV-Me₂** was constructed with two methyl groups at the former chiral center, and consequently, both of these analogues are achiral. Structures **III-[H,Me]-R** and **III-[H,Me]-S** retained the chirality present in carvedilol. Analogues **II-H₂** and **II-Me₂** were con-

Figure 3. Complete molecular structure and function of N-protonated carvedilol indicating all 11 torsional angles (top) and its three characteristic fragments: *R*- and *S*-4-(2-hydroxypropoxy)carbazol (fragment A), *R*- and *S*-*N*-ethylpropane (fragment B), and *N*-ethoxy-2-methoxybenzene (fragment C).

structed in the same manner as **IV-H$_2$** and **IV-Me$_2$** with the exception that the carbazole ring was maintained. As such, **II-H$_2$** and **II-Me$_2$** are achiral representative structures of **I-R** and **I-S**.

It is stated above that both enantiomers of carvedilol have equal α_1-adrenergic antagonist and antioxidant activities. Given the prochiral and chiral structures in Figure 4, it is of interest to ask the question, if two enantiomers produce the same biological activity (as with carvedilol), would it be possible to construct prochiral analogues of these enantiomers that could produce the same biological effects? That is, could achiral structures by synthesized that in some way could "mimic" the effects of chiral structures in a biological environment? Here, we explore such an idea with the structures presented in Figure 4.

In analyzing the various achiral and chiral structures, it is hypothesized that, with regard to conformational energies, the addition of two chiral structures, minus the addition of two achiral structures, would give a result of zero. That is, the sum of the enantiomeric *R* and *S* conformational energies would be negated by the sum of the conformational energies of the corresponding prochiral structures. This process is shown in Figure 5. How such a summation or comparison of analogous prochiral and chiral structures relates to mode of action is not fully clear (cf. Results and Discussion). However, because the complete conformational energies of a PEHS (instead of just selected conformations) comprise all structural and chiral features for a given structure, it allows us to investigate how conformational energy varies with respect to stereocenter molecular architecture. Such effects may be useful to investigate possible situations where, given the right type of molecular environment, achiral drugs could be used to "mimic" chiral compounds.

2. Computational Method

All computations were performed using the Gaussian 98 software program,[23] and all structures were exclusively defined using the Gaussian 98 z-matrix internal coordinate system to specify molecular structure, stereochemistry, and geometry. Structural analysis was done on optimized conformational minima for the respective **IV-H$_2$**, **IV-Me$_2$**, **III-[H,Me]-S**, **III-[H,Me]-R**, **I-R**, and **I-S** PEHSs. PEHSs were selected and evaluated successively at the RHF/3-21G and RHF/6-31G(d) levels of theory, and then full optimizations were carried out using the Becke 3LYP hybrid functional at the B3LYP/6-31G-(d) level of theory.[24] Separate vibrational frequency calculations were performed on all converged minima at the B3LYP/6-31G-(d) level of theory to ensure that the optimized conformers were true minima and contained no imaginary frequencies. Potential energy surfaces (PESs) were constructed according to eq 3 for **IV-H$_2$**, **IV-Me$_2$**, **III-[H,Me]-S**, **III-[H,Me]-R**, **II-H$_2$**, **II-Me$_2$**, **I-R**, and **I-S** from potential energy curve (PEC) cross sections calculated at the RHF/3-21G level of theory and plotted using Axum 5.0.[25]

$$E = f(\chi_3, \chi_{10}) \tag{3}$$

3. Results and Discussion

3.1. Enantiomeric Analysis of the I-R and I-S Torsional Angles. PEC cross sections for each torsional angle of **I-R** and **I-S** (χ_1, χ_2, χ_3, and χ_{10}) were computed using the RHF/3-21G level of theory. Given that these two structures are enantiomeric, it would be expected that each torsional mode of rotation is also enantiomeric. The latter was verified; the PECs generated

2-methoxyethan-1-ol
(analogue **IV-H$_2$**)

1-methoxy-2-methyl-propane-2-ol
(analogue **IV-Me$_2$**)

χ_2 = C5-C4-O3-C2
χ_3 = O6-C5-C4-O3
χ_{10} = H7-O6-C5-C4

(2*S*)-1-methoxypropan-2-ol
(analogue **III-[H,Me]-*S***)

(2*R*)-1-methoxypropan-2-ol
(analogue **III-[H,Me]-*R***)

E = f(χ_2, χ_3, χ_{10},)

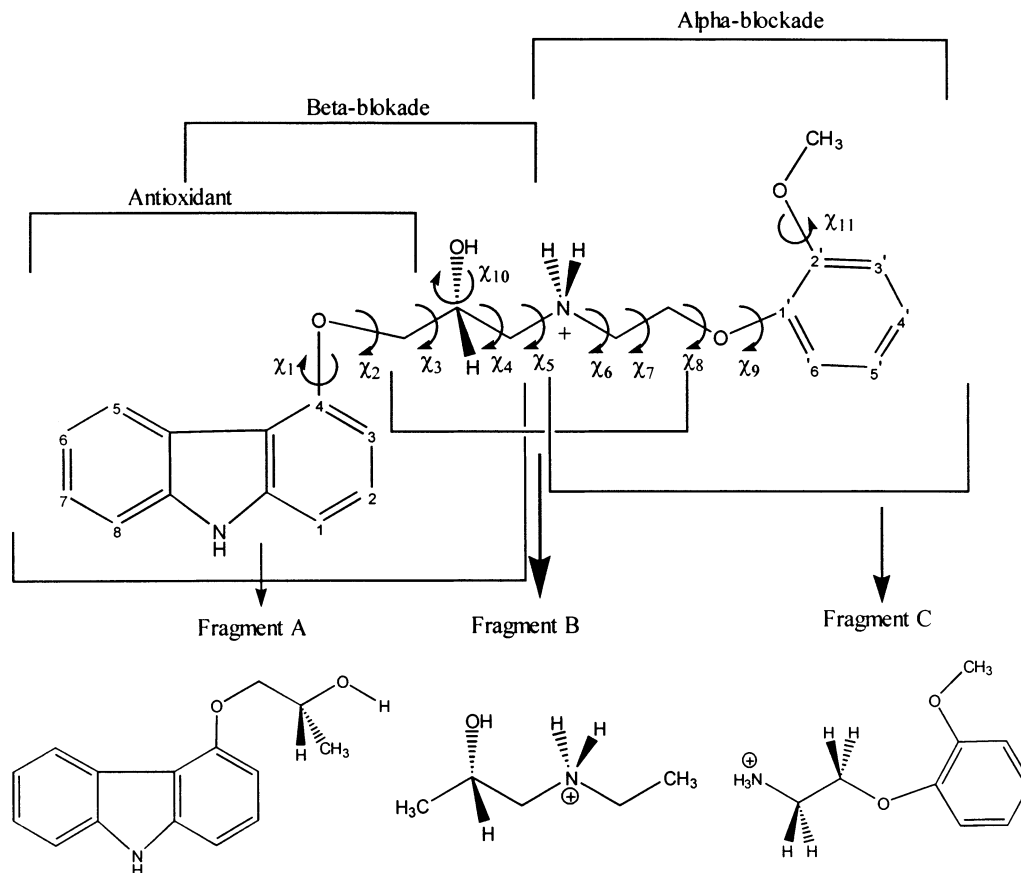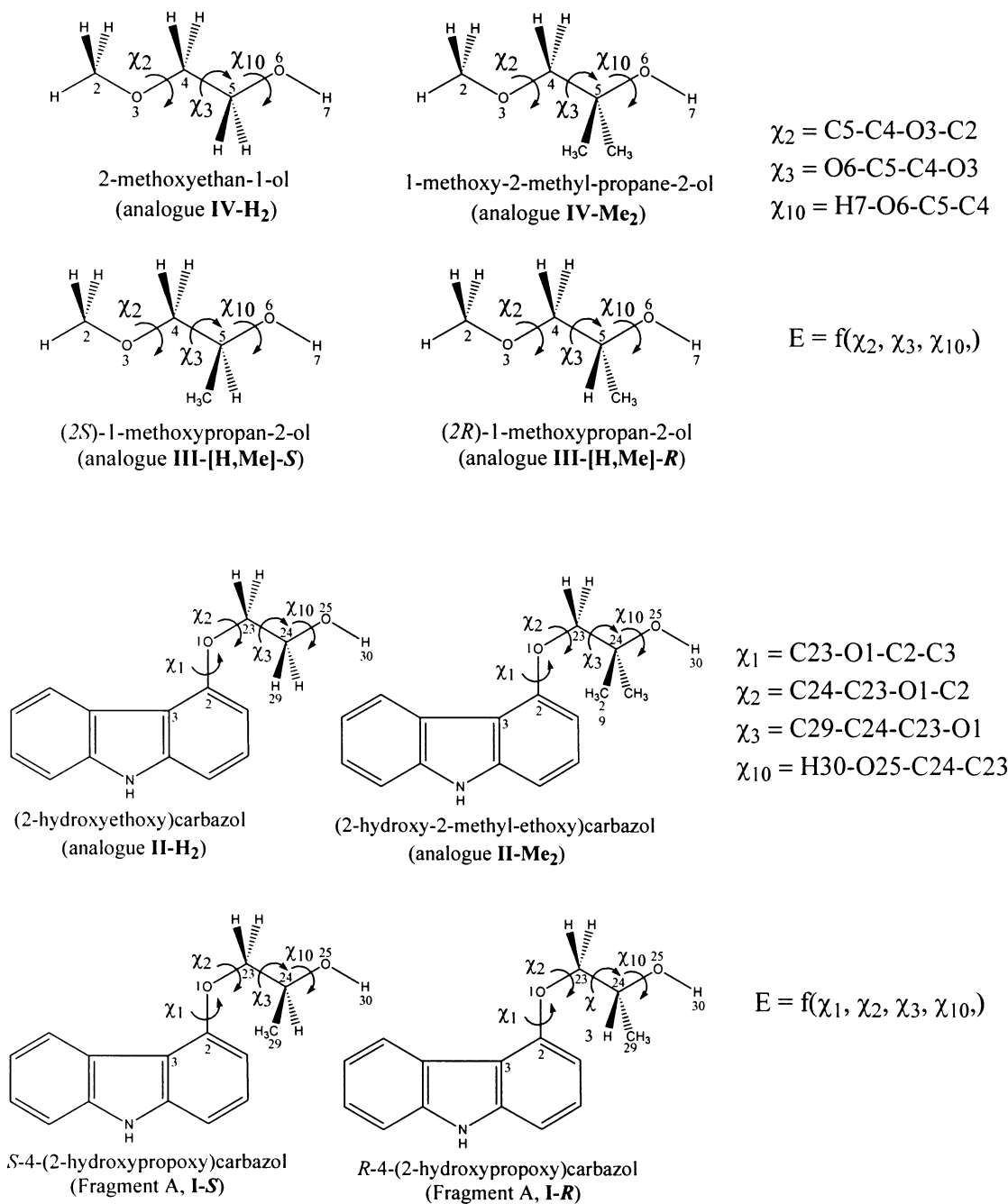(2-hydroxyethoxy)carbazol
(analogue **II-H$_2$**)

(2-hydroxy-2-methyl-ethoxy)carbazol
(analogue **II-Me$_2$**)

χ_1 = C23-O1-C2-C3
χ_2 = C24-C23-O1-C2
χ_3 = C29-C24-C23-O1
χ_{10} = H30-O25-C24-C23

S-4-(2-hydroxypropoxy)carbazol
(Fragment A, **I-*S***)

R-4-(2-hydroxypropoxy)carbazol
(Fragment A, **I-*R***)

E = f(χ_1, χ_2, χ_3, χ_{10},)

Figure 4. Numbering and definition of torsional angles for analogues **IV-H$_2$**, **IV-Me$_2$**, **III-[H,Me]-*S***, **III-[H,Me]-*R***, **II-H$_2$**, **II-Me$_2$**, **I-*R***, and **I-*S***. Numbers placed beside atoms indicate numbering used as the z-matrix input for Gaussian 98.

Chiral
(*S*-configuration)

Chiral
(*R*-configuration)

Achiral

Achiral
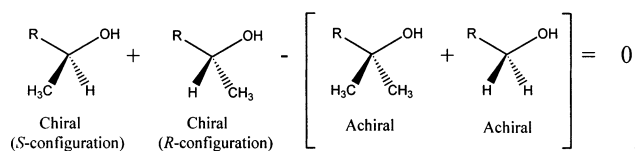
Figure 5. Calculation of the energetic equivalence of two consecutive and concerted methyl substitutions as described by $\Delta E = \{[E_R(>\text{CHMe}) + E_S(>\text{CMeH})] - [E(>\text{CMe}_2) + E(>\text{CH}_2)]\}$.

for the specified torsional angles produced topological representations of the fragment's conformational identity showing that the two structures are truly enantiomeric (cf. Figure 6). Symmetry symbols are used to identify identical points for a given torsional angle PEC. Each PEC was produced with the other three torsional angles frozen in the anti position (180.00°) to ensure no confounding factors (such as sterics) were present

for any of the torsional angles and that a controlled scan of the torsional angle was obtained. As such, the only variable in each PEC is the torsional angle being scanned because all other torsional parameters are kept rigid.

From the evaluated PECs one could estimate that the global minima for the 4-(2-hydroxypropoxy)carbazol carvedilol fragment would occur at the conformation with the torsional angles χ_1, χ_2, χ_3, and χ_{10} in the anti, anti, *g*+, *g*+ and anti, anti, *g*−, *g*− for the *R*- and *S*-configurations, respectively. This was inferred by examining the location of the global minimum for each torsional angle (χ_1, χ_2, χ_3, and χ_{10}) from each individual generated PEC.

3.2. Enantiomeric Analysis of the I-*R* and I-*S* Conformational PEHSs. After verifying that each torsional angle of the carvedilol fragment was enantiomeric, the entire PEHS described by eq 1 was analyzed by optimizations of conformational

Enantiomeric Relationships of Carvedilol Fragment A

J. Phys. Chem. A, Vol. 107, No. 29, 2003 **5599**
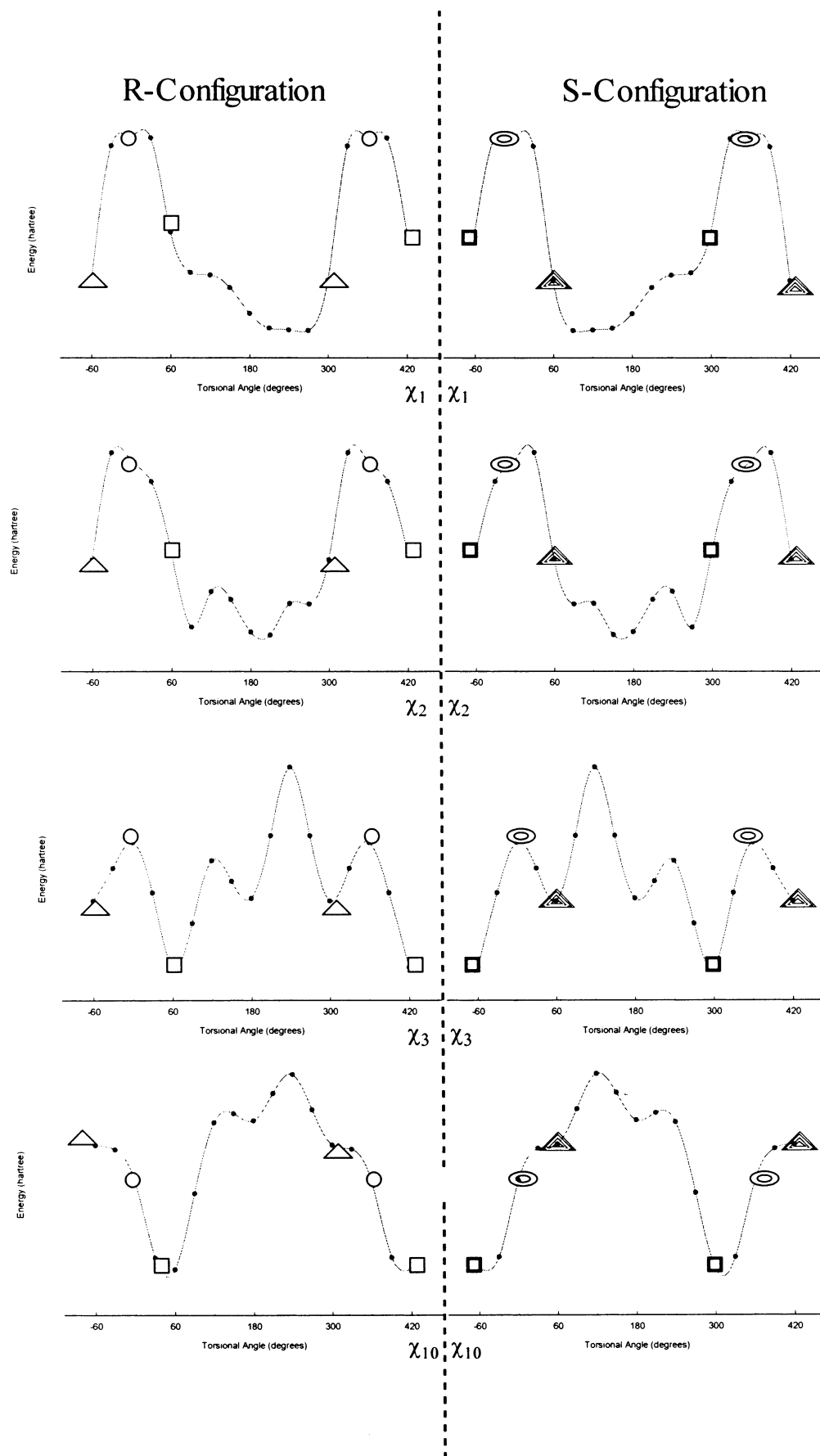
Figure 6. Enantiomeric PECs for *R*- and *S*-4-(2-hydroxypropoxy)carbazol computed at the RHF/3-21G level of theory. PECs generated for scanned torsional angles were produced with the other three torsional angles rigid at the anti position. PEC symmetry identification points are depicted by △ = gauche minus (*g*−), ○ = zero point, and □ = gauche plus (*g*+) for the *R*-configuration and □ = gauche minus (*g*−), circle in a circle = zero point, and triangle in a triangle = gauche plus (*g*+) for the *S*-configuration.

TABLE 1: Summary of Converged Conformational Minima for the PEHS of *S*-4-(2-Hydroxypropoxy)carbazol (Fragment A, I-*S*) at the RHF/3-21G [A], RHF/6-31G(d) [B], and B3LYP/6-31G(d) [C][26] Levels of Theory[a]

conformational assignment				level of theory			conformational assignment				level of theory			conformational assignment				level of theory		
χ_1	χ_2	χ_3	χ_{10}	A	B	C	χ_1	χ_2	χ_3	χ_{10}	A	B	C	χ_1	χ_2	χ_3	χ_{10}	A	B	C
g+	g+	g+	g+	F	F	F	a	g+	g+	g+	F	NF	NF	g−	g+	g+	g+	NF	NF	NF
g+	g+	g+	a	NF	NF	NF	a	g+	g+	a	NF	NF	NF	g−	g+	g+	a	NF	NF	NF
g+	g+	g+	g−	NF	NF	NF	a	g+	g+	g−	F	NF	NF	g−	g+	g+	g−	NF	NF	NF
g+	g+	a	g+	NF	NF	NF	a	g+	a	g+	NF	NF	NF	g−	g+	a	g+	NF	NF	NF
g+	g+	a	a	F	F	F	a	g+	a	a	F	F	F	g−	g+	a	a	F	NF	NF
g+	g+	a	g−	F	F	F	a	g+	a	g−	F	F	F	g−	g+	a	g−	NF	NF	NF
g+	g+	g−	g+	NF	NF	NF	a	g+	g−	g+	NF	NF	NF	g−	g+	g−	g+	NF	NF	NF
g+	g+	g−	a	NF	NF	NF	a	g+	g−	a	NF	NF	NF	g−	g+	g−	a	NF	NF	NF
g+	g+	g−	g−	NF	NF	NF	a	g+	g−	g−	NF	NF	NF	g−	g+	g−	g−	NF	NF	NF
g+	a	g+	g+	F	F	NF	a	a	g+	g+	F	F	F	g−	a	g+	g+	F GM	F	F
g+	a	g+	a	NF	NF	NF	a	a	g+	a	NF	NF	NF	g−	a	g+	a	F	F	NF
g+	a	g+	g−	NF	NF	NF	a	a	g+	g−	NF	NF	NF	g−	a	g+	g−	F	NF	NF
g+	a	a	g+	F	NF	NF	a	a	a	g+	F	F	F	g−	a	a	g+	F	F	NF
g+	a	a	a	NF	NF	NF	a	a	a	a	NF	NF	NF	g−	a	a	a	NF	NF	NF
g+	a	a	g−	F	F	F	a	a	a	g−	F	F GM	F GM	g−	a	a	g−	F	F	NF
g+	a	g−	g+	F	F	NF	a	a	g−	g+	F	F	F	g−	a	g−	g+	F	F	NF
g+	a	g−	a	NF	NF	NF	a	a	g−	a	F	F	F	g−	a	g−	a	F	F	NF
g+	a	g−	g−	NF	NF	NF	a	a	g−	g−	F	F	F	g−	a	g−	g−	F	F	NF
g+	g−	g+	g+	NF	NF	NF	a	g−	g+	g+	NF	NF	NF	g−	g−	g+	g+	NF	NF	NF
g+	g−	g+	a	NF	NF	NF	a	g−	g+	a	F	NF	NF	g−	g−	g+	a	F	NF	NF
g+	g−	g+	g−	NF	NF	NF	a	g−	g+	g−	NF	NF	NF	g−	g−	g+	g−	NF	NF	NF
g+	g−	a	g+	NF	NF	NF	a	g−	a	g+	F	NF	NF	g−	g−	a	g+	NF	NF	NF
g+	g−	a	a	NF	NF	NF	a	g−	a	a	F	F	F	g−	g−	a	a	NF	NF	NF
g+	g−	a	g−	NF	NF	NF	a	g−	a	g−	F	NF	NF	g−	g−	a	g−	F	F	F
g+	g−	g−	g+	NF	NF	NF	a	g−	g−	g+	F	F	F	g−	g−	g−	g+	NF	NF	NF
g+	g−	g−	a	NF	NF	NF	a	g−	g−	a	F	F	F	g−	g−	g−	a	NF	NF	NF
g+	g−	g−	g−	NF	NF	NF	a	g−	g−	g−	F	F	F	g−	g−	g−	g−	F	F	F

[a] F = found; NF = not found; GM = global minimum.

minima. With four torsional angles (χ_1, χ_2, χ_3, χ_{10}) and three possible minima for each torsional angle (g+, a, g−), there are a grand total of 81 (=3^4) possible minima for each configuration. Minima are indicated as either $\chi_1[\chi_2\chi_3]\chi_{10}$ or $[\chi_2\chi_3]\chi_{10}$ because the torsional angles χ_2 and χ_3 are reflective of the backbone conformation assumed by carvedilol fragment A.

Conformational structural assignments for the conformational minima were made using the following conditions:

$$\text{gauche plus (g+)} = 60 \text{ (ideal)} \pm 60°$$

$$\text{anti (a)} = 180 \text{ (ideal)} \pm 60°$$

$$\text{gauche minus (g−)} = -60 \text{ (ideal)} \pm 60°$$

This is based on the general observation that, if one were to rotate a tetrahedral carbon against another tetrahedral carbon, the minima would generally fall within the above ranges. All possible minima were computed at noncorrelated Hartree−Fock RHF/3-21G, subsequent minima at RHF/6-31G(d), and then using the density functional hybrid B3LYP/6-31G(d). Minima were then sorted according to the above conformational assignments and were either termed found (F) if they converged or not found (NF) if the structure shifted to nearby minima or was annihilated due to lack of stability at a specific conformation. Tables 1 and 2 show a summary of all the converged PEHS conformers at all levels of theory for **I-*S*** and **I-*R***, respectively. The B3LYP/6-31G(d) results in column C of Table 1 are adapted from ref 26.

The number of minima found for **I-*S*** and **I-*R*** are, respectively, 36 minima converged (the global minima were the g−[ag+]g+ and g+[ag−]g− conformations) at RHF/3-21G (cf. Supporting Information Tables S1 and S2), 27 minima (a[aa]g− and a[aa]g+) at RHF/6-31G(d) (cf. Supporting Information Tables S3 and S4), and 19 minima (a[aa]g− and a[aa]g+) at B3LYP/6-31G(d) (cf. ref 26 for **I-*S*** and Table 3 for **I-*R***).

Minima were stabilized by intramolecular hydrogen bonding between O1 and H30.[26]

All converged minima at the B3LYP/6-31G(d) level of theory that were concluded to be authentic minima (i.e. possessed no imaginary frequencies) were used to construct a topological representation of the PEHS for **I-*S*** and **I-*R*** (cf. Figure 7). From this schematic diagram, it is evident that all minima occurred in corresponding enantiomeric pairs. Further, the PEHS generated for both stereoisomers illustrates that both the *R*- and *S*-configurations possess both point chirality and axis chirality and are exactly enantiomeric, as described by eq 4.

$$E_R = E_S \qquad (4)$$

$$f_R(\chi_1, \chi_2, \chi_3, \chi_{10}) = f_S(-\chi_1, -\chi_2, -\chi_3, -\chi_{10})$$

It is therefore evident that in the present molecular system we are witnessing the combination of both point chirality and axis chirality. Consequently, a true enantiomeric pair requires not only the switching of point chirality from the *R*- to the *S*-stereoisomer but also the switching of all torsional angles from clockwise (CW) to counterclockwise (CCW) rotation, as demanded by eq 4. Consequently, the graphical representation of the computed PEHS shows that all minima must have an energetically equal enantiomer (as described in eq 4). All other pairs have diastereomeric relationships. This observation is valid for all three levels of theory employed for all conformational optimizations. The above is also schematically illustrated in Figure 1.

DFT global minima, a[aa]g− and a[aa]g+ for the *S*- and *R*-configurations, respectively, reveal that the initial guesses of a[ag−]g− and a[ag+]g+ for global minima obtained from the RHF/3-21G PECs were quite close to the final DFT converged global minima. In fact, these PEC-based predictions were closer

TABLE 2: Summary of Converged Conformational Minima for the PEHS of *R*-4-(2-Hydroxypropoxy)carbazol (Fragment A, I-*R*) at the RHF/3-21G [A], RHF/6-31G(d) [B], and B3LYP/6-31G(d) [C] Levels of Theory[a]

conformational assignment				level of theory			conformational assignment				level of theory			conformational assignment				level of theory		
χ_1	χ_2	χ_3	χ_{10}	A	B	C	χ_1	χ_2	χ_3	χ_{10}	A	B	C	χ_1	χ_2	χ_3	χ_{10}	A	B	C
g^+	g^+	g^+	g^+	F	F	F	a	g^+	g^+	g^+	F	F	F	g^-	g^+	g^+	g^+	NF	NF	NF
g^+	g^+	g^+	a	NF	NF	NF	a	g^+	g^+	a	F	F	F	g^-	g^+	g^+	a	NF	NF	NF
g^+	g^+	g^+	g^-	NF	NF	NF	a	g^+	g^+	g^-	F	F	F	g^-	g^+	g^+	g^-	NF	NF	NF
g^+	g^+	a	g^+	F	F	F	a	g^+	a	g^+	F	NF	NF	g^-	g^+	a	g^+	NF	NF	NF
g^+	g^+	a	a	NF	NF	NF	a	g^+	a	a	F	F	F	g^-	g^+	a	a	NF	NF	NF
g^+	g^+	a	g^-	NF	NF	NF	a	g^+	a	g^-	F	NF	NF	g^-	g^+	a	g^-	NF	NF	NF
g^+	g^+	g^-	g^+	NF	NF	NF	a	g^+	g^-	g^+	NF	NF	NF	g^-	g^+	g^-	g^+	NF	NF	NF
g^+	g^+	g^-	a	F	NF	NF	a	g^+	g^-	a	F	NF	NF	g^-	g^+	g^-	a	NF	NF	NF
g^+	g^+	g^-	g^-	NF	NF	NF	a	g^+	g^-	g^-	NF	NF	NF	g^-	g^+	g^-	g^-	NF	NF	NF
g^+	a	g^+	g^+	F	F	NF	a	a	g^+	g^+	F	F	F	g^-	a	g^+	g^+	NF	NF	NF
g^+	a	g^+	a	F	F	NF	a	a	g^+	a	F	F	F	g^-	a	g^+	a	NF	NF	NF
g^+	a	g^+	g^-	F	F	NF	a	a	g^+	g^-	F	F	F	g^-	a	g^+	g^-	F	F	NF
g^+	a	a	g^+	F	F	NF	a	a	a	g^+	F	F GM	F GM	g^-	a	a	g^+	F	F	F
g^+	a	a	a	NF	NF	NF	a	a	a	a	NF	NF	NF	g^-	a	a	a	NF	NF	NF
g^+	a	a	g^-	F	F	NF	a	a	a	g^-	F	F	F	g^-	a	a	g^-	F	NF	NF
g^+	a	g^-	g^+	F	NF	NF	a	a	g^-	g^+	NF	NF	NF	g^-	a	g^-	g^+	NF	NF	NF
g^+	a	g^-	a	F	F	NF	a	a	g^-	a	NF	NF	NF	g^-	a	g^-	a	NF	NF	NF
g^+	a	g^-	g^-	F GM	F	F	a	a	g^-	g^-	F	F	F	g^-	a	g^-	g^-	F	F	NF
g^+	g^-	g^+	g^+	NF	NF	NF	a	g^-	g^+	g^+	F	F	F	g^-	g^-	g^+	g^+	NF	NF	NF
g^+	g^-	g^+	a	NF	NF	NF	a	g^-	g^+	a	NF	NF	NF	g^-	g^-	g^+	a	NF	NF	NF
g^+	g^-	g^+	g^-	NF	NF	NF	a	g^-	g^+	g^-	NF	NF	NF	g^-	g^-	g^+	g^-	NF	NF	NF
g^+	g^-	a	g^+	NF	NF	NF	a	g^-	a	g^+	F	F	F	g^-	g^-	a	g^+	F	F	F
g^+	g^-	a	a	F	NF	NF	a	g^-	a	a	F	F	F	g^-	g^-	a	a	F	F	F
g^+	g^-	a	g^-	NF	NF	NF	a	g^-	a	g^-	NF	NF	NF	g^-	g^-	a	g^-	NF	NF	NF
g^+	g^-	g^-	g^+	NF	NF	NF	a	g^-	g^-	g^+	F	NF	NF	g^-	g^-	g^-	g^+	NF	NF	NF
g^+	g^-	g^-	a	NF	NF	NF	a	g^-	g^-	a	NF	NF	NF	g^-	g^-	g^-	a	NF	NF	NF
g^+	g^-	g^-	g^-	NF	NF	NF	a	g^-	g^-	g^-	F	NF	NF	g^-	g^-	g^-	g^-	F	F	F

[a] F = found; NF = not found; GM = global minimum.

TABLE 3: Optimized Minima for the PEHS of *R*-4-(2-Hydroxypropoxy)carbazol (Fragment A, I-*R*) at the B3LYP/6-31G(d) Level of Theory

conformational assignment									
χ_1	χ_2	χ_3	χ_{10}	χ_1	χ_2	χ_3	χ_{10}	*E* (hartree)	rel *E* (kcal·mol^{-1})
g^+	g^+	g^+	g^+	78.66	85.51	64.48	66.64	−785.828 425 897	6.34
g^+	g^+	a	g^+	74.44	80.27	166.22	58.86	−785.830 399 472	5.11
g^+	a	g^-	g^-	84.56	−176.64	−68.86	−53.52	−785.834 927 568	2.26
a	g^+	g^+	g^+	−179.82	82.40	61.44	68.99	−785.832 614 704	3.72
a	g^+	g^+	a	−179.85	82.74	62.70	−175.60	−785.833 159 064	3.37
a	g^+	g^+	g^-	−179.33	81.90	58.61	−74.35	−785.833 289 337	3.29
a	g^+	a	a	156.09	105.16	163.35	167.64	−785.831 784 831	4.24
a	a	g^+	g^+	−178.82	−179.20	66.89	68.63	−785.834 719 251	2.40
a	a	g^+	a	179.99	−178.34	65.45	−176.78	−785.834 841 115	2.32
a	a	g^+	g^-	−179.64	−178.70	62.36	−75.51	−785.834 880 226	2.29
a	a	a	g^+	−178.53	175.39	−178.18	47.53	−785.838 535 919	0.00
a	a	a	g^-	−175.20	−177.94	−179.89	−56.46	−785.833 846 146	2.94
a	a	g^-	g^-	177.68	−176.27	−65.84	−50.64	−785.837 142 473	0.87
a	g^-	a	g^+	−178.26	−86.25	−174.77	49.15	−785.836 187 425	1.47
a	g^-	a	a	177.86	−80.88	172.56	168.92	−785.831 134 398	4.64
g^-	a	a	g^+	−83.67	176.13	−173.69	50.76	−785.836 021 086	1.58
g^-	g^-	a	g^+	−87.09	−84.22	−171.18	37.39	−785.832 806 928	3.60
g^-	g^-	a	a	−85.33	−66.15	−179.25	177.98	−785.827 602 283	6.86
g^-	g^-	g^-	g^-	−71.75	−86.37	−54.09	−60.91	−785.829 262 278	5.82

to the DFT global minima than to the global minima from the RHF/3-21G conformational optimizations. This is likely due to the fact that the PECs were constructed with the three other torsional angles rigid, allowing good topological profiles to be generated for each torsional angle without confounding factors from the other torsional angles.

3.3. PEHS Conformational Analysis of IV-H₂, IV-Me₂, III-[H,Me]-*S*, and III-[H,Me]-*R*. Selected analogues were subject to the same conformational structural assignments and optimization methods as described above for **I-*S*** and **I-*R***. A summary of the converged minima for **IV-H₂** is found in Table 4. This analogue contains two equivalent global minima at [a*g*+]*g*− and [a*g*−]*g*+ (cf. Figure 8 and Table 5) that converged at all

three levels of theory (cf. Supporting Information Tables S5 and S6). **I-*S*** and **I-*R***, which were strained by the large carbazole ring substituent, had fewer numbers of minima converge at each level of theory. The simple methyl substituent, along with only two hydrogen atoms present at carbon center C5, produced a PEHS with 21 converged minima out of a possible 27 for each different level of theory. Due to the latter, although a larger basis set and the DFT level of theory produced better energies, the PEHS remained relatively unchanged for the three levels of geometry optimizations.

The other noncarbazole achiral analogue, **IV-Me₂**, was also analyzed with geometry optimizations (cf. Table 6). This analogue was identical to **IV-H₂** with the exception that C5
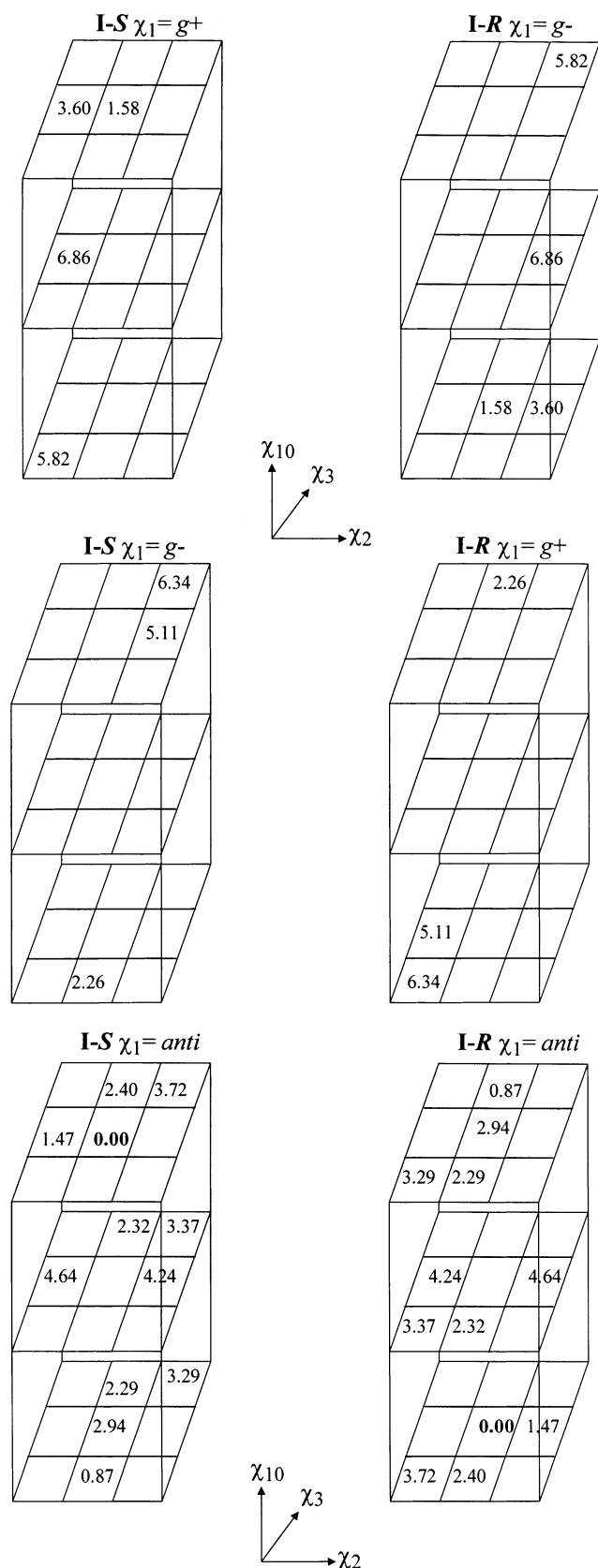
Figure 7. Graphical representation of the density functional computed PEHSs for *R*- and *S*-4-(2-hydroxypropoxy)carbazol (**I-R** and **I-S**) indicating all minima found and the associated relative energy in kcal·mol⁻¹. Minima that were not found have a blank space.

contained two methyl substituents as opposed to two hydrogen atoms. Like the case of **IV-H₂**, two energetically identical global minima occurred at the conformations [*ag*+]*g*− and [*ag*−]*g*+

TABLE 4: Summary of Converged Conformational Minima for the PEHS of 2-Methoxyethan-1-ol (IV-H₂) at the RHF/3-21G [A], RHF/6-31G(d) [B], and B3LYP/6-31G(d) [C] Levels of Theory[a]

conformational assignment					
χ_2	χ_3	χ_{10}	A	B	C
g⁺	g⁺	g⁺	NF	NF	NF
g⁺	g⁺	a	F	F	F
g⁺	g⁺	g⁻	F	F	F
g⁺	a	g⁺	F	F	F
g⁺	a	a	F	F	F
g⁺	a	g⁻	F	F	F
g⁺	g⁻	g⁺	NF	NF	NF
g⁺	g⁻	a	F	F	F
g⁺	g⁻	g⁻	F	F	F
a	g⁺	g⁺	F	F	F
a	g⁺	a	NF	NF	NF
a	g⁺	g⁻	F (GM)	F (GM)	F (GM)
a	a	g⁺	F	F	F
a	a	a	F	F	F
a	a	g⁻	F	F	F
a	g⁻	g⁺	F (GM)	F (GM)	F (GM)
a	g⁻	a	NF	NF	NF
a	g⁻	g⁻	F	F	F
g⁻	g⁺	g⁺	F	F	F
g⁻	g⁺	a	F	F	F
g⁻	g⁺	g⁻	NF	NF	NF
g⁻	a	g⁺	F	F	F
g⁻	a	a	F	F	F
g⁻	a	g⁻	F	F	F
g⁻	g⁻	g⁺	F	F	F
g⁻	g⁻	a	F	F	F
g⁻	g⁻	g⁻	NF	NF	NF

[a] F = found; NF = not found; GM = global minimum.

for all three different levels of theory (cf. Figure 9 and Table 7). However, due to the steric restrictions imposed by the somewhat larger methyl groups at C5, only 11 out of the possible 27 minima converged at the different levels of optimization (cf. Supporting Information Tables S7 and S8). The presence of the methyl groups prevented most of the conformations with the torsional angle χ_2 in the *g*+ or *g*− position from converging.

Here too we witness the presence of axis chirality in these achiral (with regards to point chirality) structures. Therefore, although these achiral structures will not rotate plane-polarized light as point chiral structures do, they possess axis chirality which occurs when the structures adopt conformations with asymmetric electron density planes. The only exception to this is the [*aa*]*a* conformation. This conformation separates all minima for a given structure because it is the only conformation with a symmetric electron density plane, and therefore, axis chirality is not present—consequently, it does not have an axis chiral pair. However, conformations above and below the [*aa*]*a* conformation are influenced by axis chirality and are paired according to eq 5. Equation 5 states that for an achiral structure with two energetically equivalent minima, P and M, all torsional angles for those minima are switched from clockwise (CW) to counterclockwise (CCW) rotation. This axis chirality is the same as that demanded by eq 4 for the two enantiomeric minima.

$$E_P = E_M \qquad (5)$$

$$f_P(\chi_2,\chi_3,\chi_{10}) = f_M(-\chi_2,-\chi_3,-\chi_{10})$$

It must be regarded that, as stated earlier, irrespective of the presence of a point chiral stereocenter with four different

Enantiomeric Relationships of Carvedilol Fragment A

J. Phys. Chem. A, Vol. 107, No. 29, 2003 **5603**

TABLE 5: Optimized Minima for the PEHS of 2-Methoxyethan-1-ol (IV-H$_2$) at the B3LYP/6-31G(d) Level of Theory

conformational assignment			χ_2	χ_3	χ_{10}	E (hartree)	rel E (kcal·mol^{-1})
χ_2	χ_3	χ_{10}					
g^+	g^+	a	74.84	64.71	−176.35	−269.542 422 374	5.34
g^+	g^+	g^-	84.22	55.17	−43.31	−269.548 526 782	1.51
g^+	a	g^+	82.10	176.20	67.87	−269.543 841 268	4.45
g^+	a	a	83.07	178.41	−177.30	−269.543 541 796	4.63
g^+	a	g^-	81.30	178.57	−67.44	−269.544 279 753	4.17
g^+	g^-	a	81.32	−75.42	173.05	−269.545 157 695	3.62
g^+	g^-	g^-	78.24	−71.37	−63.90	−269.545 185 796	3.60
a	g^+	g^+	−178.77	64.47	58.69	−269.544 928 112	3.76
a	g^+	g^-	−173.81	59.60	−49.85	−269.550 927 094	0.00
a	a	g^+	−178.30	179.68	69.45	−269.546 263 161	2.93
a	a	a	180.00	180.00	180.00	−269.545 824 036	3.20
a	a	g^-	178.30	−179.67	−69.48	−269.546 263 144	2.93
a	g^-	g^+	173.81	−59.60	49.85	−269.550 927 095	0.00
a	g^-	g^-	178.77	−64.47	−58.69	−269.544 928 111	3.76
g^-	g^+	g^+	−78.24	71.37	63.90	−269.545 185 796	3.60
g^-	g^+	a	−81.32	75.42	−173.04	−269.545 157 695	3.62
g^-	a	g^+	−81.30	−178.57	67.44	−269.544 279 753	4.17
g^-	a	a	−83.07	−178.41	177.30	−269.543 541 796	4.63
g^-	a	g^-	−82.10	−176.20	−67.87	−269.543 841 268	4.45
g^-	g^-	g^+	−84.23	−55.18	43.31	−269.548 526 783	1.51
g^-	g^-	a	−74.84	−64.71	176.35	−269.542 422 374	5.34

2.30

[*ag*+]*g*-

2.30

[*ag*-]*g*+
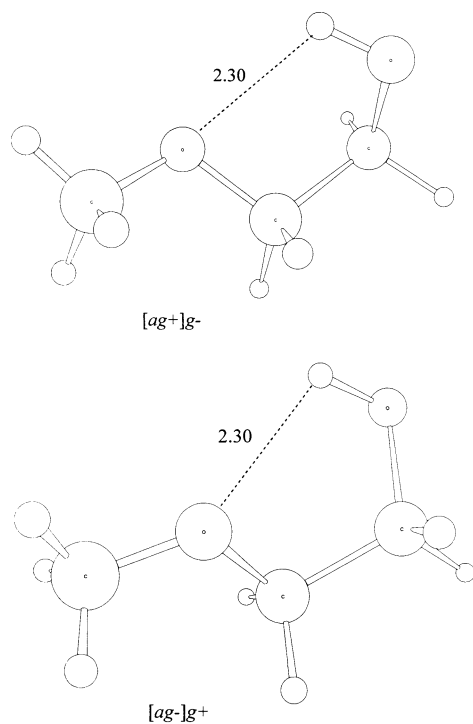
Figure 8. Global minima conformers of the 2-methoxyethan-1-ol (**IV-H$_2$**) PEHS. Conformers [*ag*+]*g*− (top) and [*ag*−]*g*+ (bottom) are axis chiral pairs computed at the B3LYP/6-31G(d) level of theory and possess an intramolecular hydrogen bond as the dominant stabilization feature.

TABLE 6: Summary of Converged Conformational Minima for the PEHS of 1-Methoxy-2-methyl-propane-2-ol (IV-Me$_2$) at the RHF/3-21G [A], RHF/6-31G(d) [B], and B3LYP/6-31G(d) [C] Levels of Theory^a

conformational assignment			A	B	C
χ_2	χ_3	χ_{10}			
g^+	g^+	g^+	NF	NF	NF
g^+	g^+	a	NF	NF	NF
g^+	g^+	g^-	NF	NF	NF
g^+	a	g^+	NF	NF	NF
g^+	a	a	NF	NF	NF
g^+	a	g^-	NF	NF	NF
g^+	g^-	g^+	NF	NF	NF
g^+	g^-	a	F	F	F
g^+	g^-	g^-	F	F	F
a	g^+	g^+	NF	NF	NF
a	g^+	a	F	F	F
a	g^+	g^-	F (GM)	F (GM)	F (GM)
a	a	g^+	F	F	F
a	a	a	F	F	F
a	a	g^-	F	F	F
a	g^-	g^+	F (GM)	F (GM)	F (GM)
a	g^-	a	F	F	F
a	g^-	g^-	NF	NF	NF
g^-	g^+	g^+	F	F	F
g^-	g^+	a	F	F	F
g^-	g^+	g^-	NF	NF	NF
g^-	a	g^+	NF	NF	NF
g^-	a	a	NF	NF	NF
g^-	a	g^-	NF	NF	NF
g^-	g^-	g^+	NF	NF	NF
g^-	g^-	a	NF	NF	NF
g^-	g^-	g^-	NF	NF	NF

^{a} F = found; NF = not found; GM = global minimum.

substituents, the chirality induced by an asymmetric distribution of electron density—axis chirality—is always present whenever the structure adopts asymmetric conformations. Further, like enantiomers of point chirality, axis chiral conformers come in pairs.

If one were to differently combine the two achiral analogues, **IV-H$_2$** and **IV-Me$_2$** at C5, one would acquire two enantiomers: **III-[H,Me]-S** and **III-[H,Me]-R** (cf. Figure 4). These two enantiomers were each evaluated with geometry optimizations of converged minima as above (cf. Tables 8 and 9). Given that

21 and 11 minima converged for the **IV-H$_2$** and **IV-Me$_2$** PEHSs, respectively, it would be expected that, with one hydrogen and one methyl group at C5, the number halfway between 11 and 21 would converge for the enantiomeric structures (i.e. (11 + 21)/2 = 16). This is exactly what occurred, with each configuration and level of theory having 16 out of a possible 27 minima converge for each enantiomer. Further, given that the global minima occurred at the [*ag*+]*g*− and [*ag*−]*g*+ conformations for the achiral structures, it would be expected that the

TABLE 7: Optimized Minima for the PEHS of 1-Methoxy-2-methyl-propane-2-ol (IV-Me$_2$) at the B3LYP/6-31G(d) Level of Theory

conformational assignment			χ_2	χ_3	χ_{10}	E (hartree)	Rel E (kcal·mol^{-1})
χ_2	χ_3	χ_{10}					
g$^+$	g$^-$	a	χ_2	χ_3	χ_{10}	−348.182 592 886	3.36
g$^+$	g$^-$	g$^-$	81.08	−67.14	−63.97	−348.182 032 926	3.71
a	g$^+$	a	−177.62	69.32	−174.14	−348.181 677 861	3.94
a	g$^+$	g$^-$	−174.24	55.90	−46.46	−348.187 950 829	0.00
a	a	g$^+$	−178.29	179.67	70.72	−348.184 592 291	2.11
a	a	a	180.00	−179.98	−179.95	−348.184 521 481	2.15
a	a	g$^-$	178.29	−179.67	−70.72	−348.184 592 292	2.11
a	g$^-$	g$^+$	174.24	−55.90	46.46	−348.187 950 829	0.00
a	g$^-$	a	177.62	−69.32	174.15	−348.181 677 884	3.94
g$^-$	g$^+$	g$^+$	−81.08	67.13	63.97	−348.182 032 924	3.71
g$^-$	g$^+$	a	−86.20	71.30	−174.64	−348.182 592 888	3.36

2.19

[ag+]g-

2.19

[ag-]g+
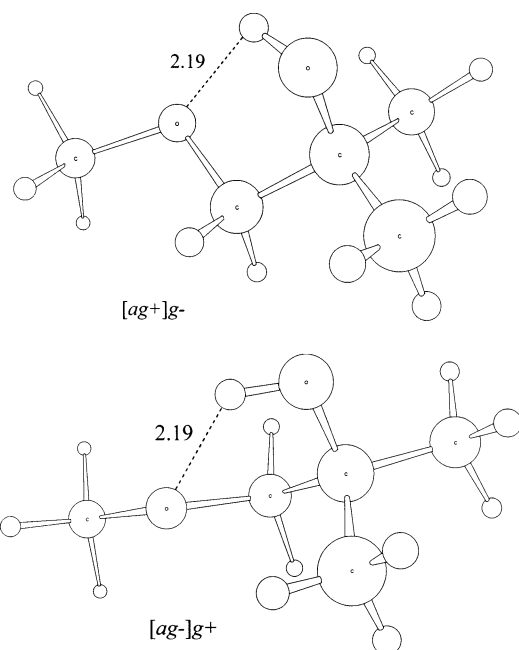
Figure 9. Global minima conformers of the 1-methoxy-2-methyl-propane-2-ol (**IV-Me$_2$**) PEHSs computed at the B3LYP/6-31G(d) level of theory. Similarly to the **IV-H$_2$** PEHS, conformers [*ag*+]*g*− (top) and [*ag*−]*g*+ (bottom) are axis chiral pairs with the same intramolecular hydrogen bond as the dominant stabilization feature.

chiral enantiomers would have global minima at either of these conformations. This also occurred. However, the enantiomers varied their global minima at the RHF/3-21G and RHF/6-31G-(d) levels of theory (cf. Figure 10 and Tables 8 and 9). Also, like the cases of the achiral analogues, the PEHSs of **III-[H,-Me]-S** and **III-[H,Me]-R** stayed constant at the different levels of theory. This was contrary to the cases of the PEHSs of **I-S** and **I-R**, where the number of converged minima decreased at successive levels of theory.

Conformational analysis of **III-[H,Me]-S** and **III-[H,Me]-R** (cf. Tables 10 and 11) revealed that their respective PEHSs can be described by eq 4 and Figure 1, illustrating the presence of point and axis chirality in these enantiomers (cf. Supporting Information Tables S9−S12). Topological representations of the PEHSs were also constructed for these analogues to illustrate the above trend (cf. Figure 11). In comparing the PEHSs of **III-[H,Me]-S** and **III-[H,Me]-R** with those of **I-S** and **I-R**, one can see that the presence of the bulky carbazole ring system limits the possible conformations the carvedilol fragment can adopt. Also, like **I-S** and **I-R**, all four methyl-substituted analogues were stabilized by intramolecular hydrogen bonding

TABLE 8: Summary of Converged Conformational Minima for the PEHS of (2S)-1-Methoxypropan-2-ol (III-[H,Me]-S) at the RHF/3-21G [A], RHF/6-31G(d) [B], and B3LYP/6-31G(d) [C] Levels of Theory^a

conformational assignment			A	B	C
χ_2	χ_3	χ_{10}			
g$^+$	g$^+$	g$^+$	NF	NF	NF
g$^+$	g$^+$	a	F	F	F
g$^+$	g$^+$	g$^-$	F	F	F
g$^+$	a	g$^+$	NF	NF	NF
g$^+$	a	a	NF	NF	NF
g$^+$	a	g$^-$	NF	NF	NF
g$^+$	g$^-$	g$^+$	NF	NF	NF
g$^+$	g$^-$	a	F	F	F
g$^+$	g$^-$	g$^-$	F	F	F
a	g$^+$	g$^+$	NF	NF	NF
a	g$^+$	a	F	F	F
a	g$^+$	g$^-$	F	F (GM)	F (GM)
a	a	g$^+$	F	F	F
a	a	a	F	F	F
a	a	g$^-$	F	F	F
a	g$^-$	g$^+$	F (GM)	F	F
a	g$^-$	a	F	F	F
a	g$^-$	g$^-$	NF	NF	NF
g$^-$	g$^+$	g$^+$	F	F	F
g$^-$	g$^+$	a	F	F	F
g$^-$	g$^+$	g$^-$	NF	NF	NF
g$^-$	a	g$^+$	F	F	F
g$^-$	a	a	F	F	F
g$^-$	a	g$^-$	F	F	F
g$^-$	g$^-$	g$^+$	NF	NF	NF
g$^-$	g$^-$	a	NF	NF	NF
g$^-$	g$^-$	g$^-$	NF	NF	NF

^{a} F = found; NF = not found; GM = global minimum.

between the ether oxygen (O3) and the terminal hydroxyl hydrogen (H7) (cf. Figures 8−10).

The above discussion illustrates that the properties of achiral and chiral structures are not completely distinct (given that the only differences occur at the chiral center) and that deductions about chiral structures can be made from achiral analysis and vice versa. Also, the presence of axis chirality in an achiral system ensures that not all conformations will be unique but rather can be predicted from eq 5.

3.4. PES Analysis of the Chiral and Achiral Centers of I-R, I-S, II-H$_2$, II-Me$_2$, III-[H,Me]-S, III-[H,Me]-R, IV-H$_2$, and IV-Me$_2$. To further study the chiral and achiral centers of the carvedilol analogues, 169-point PESs were constructed from PEC cross sections of torsional angles χ_3 and χ_{10} according to eq 3 at the RHF/3-21G level of theory (cf. Computational Method). These surfaces were constructed using these two torsional angles because they directly surround the chiral and

Enantiomeric Relationships of Carvedilol Fragment A

J. Phys. Chem. A, Vol. 107, No. 29, 2003 **5605**

TABLE 9: Summary of Converged Conformational Minima for the PEHS of (2*R*)-1-Methoxypropan-2-ol (III-[H,Me]-*R*) at the RHF/3-21G [A], RHF/6-31G(d) [B], and B3LYP/ 6-31G(d) [C] Levels of Theory[a]

conformational assignment					
χ_2	χ_3	χ_{10}	A	B	C
g^+	g^+	g^+	NF	NF	NF
g^+	g^+	a	NF	NF	NF
g^+	g^+	g^-	NF	NF	NF
g^+	a	g^+	F	F	F
g^+	a	a	F	F	F
g^+	a	g^-	F	F	F
g^+	g^-	g^+	NF	NF	NF
g^+	g^-	a	F	F	F
g^+	g^-	g^-	F	F	F
a	g^+	g^+	NF	NF	NF
a	g^+	a	F	F	F
a	g^+	g^-	F (GM)	F	F
a	a	g^+	F	F	F
a	a	a	F	F	F
a	a	g^-	F	F	F
a	g^-	g^+	F	F (GM)	F (GM)
a	g^-	a	F	F	F
a	g^-	g^-	NF	NF	NF
g^-	g^+	g^+	F	F	F
g^-	g^+	a	F	F	F
g^-	g^+	g^-	NF	NF	NF
g^-	a	g^+	NF	NF	NF
g^-	a	a	NF	NF	NF
g^-	a	g^-	NF	NF	NF
g^-	g^-	g^+	F	F	F
g^-	g^-	a	F	F	F
g^-	g^-	g^-	NF	NF	NF

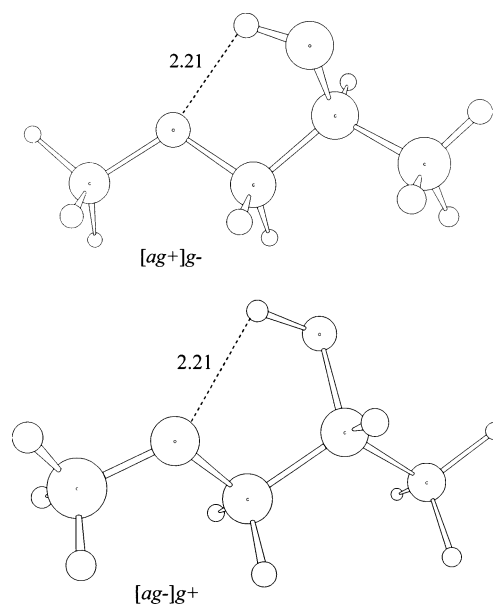[a] F = found; NF = not found; GM = global minimum.

Figure 10. Global minima conformers of the (2*S*)-1-methoxypropan-2-ol (**III-[H,Me]-*S***) and (2*R*)-1-methoxypropan-2-ol (**III-[H,Me]-*R***) PEHSs computed at the B3LYP/6-31G(d) level of theory. Conformer [*ag*+]*g*− (top) represents the **III-[H,Me]-*S*** global minimum while conformer [*ag*−]*g*+ (bottom) represents the **III-[H,Me]-*R*** global minimum. Both conformers are enantiomeric and axis chiral pairs and possess intramolecular hydrogen bonding as the dominant feature.

achiral centers and therefore provide the best representation of the behavior about these centers. Given that the rest of the structures are identical, these will allow for valid interpretations of what is occurring at C5 and C24.

All four methyl-substituted analogues were computed (cf. Figure 12). The PESs of **IV-H₂** and **IV-Me₂** illustrate the effects of having two methyl groups bonded at C5 (for the latter) versus two hydrogen atoms (for the former). The barriers of rotation for **IV-Me₂** are larger than that of **IV-H₂**, as expected. The PESs of **III-[H,Me]-*S*** and **III-[H,Me]-*R*** reveal intermediate barriers of rotation. Upon analysis of their respective contour maps, the presence of both point and axis chirality is evident, similar to the graphical representation in Figure 11.

The same methodology was applied to **II-H₂** and **II-Me₂**, which are the achiral analogues of the carbazole-containing enantiomers (cf. Figure 13). The effects of the carbazole ring substituent are seen as large maxima indicating large barriers of rotation present in all four PEHS. The double-methyl achiral structure also has larger barriers of rotation while the enantiomers have intermediate barriers due to the presence of only a single methyl at C24. Like the cases of **III-[H,Me]-*S*** and **III-[H,Me]-*R***, analysis of the contour maps for **I-*R*** and **I-*S*** reveals both point and axis chirality.

Upon construction of the PESs, the question put forth by Figure 5 was addressed: given the summation in eq 6, with two enantiomers with one stereocenter (denoted as >CHMe and >CMeH) and two corresponding achiral structures (denoted as >CMe₂ and >CH₂), would the summation of the two chiral structures cancel out the summation of the two achiral structures? In other words, would ΔE equal zero? This was tested

TABLE 10: Optimized Minima for the PEHS of (2*S*)-1-Methoxypropan-2-ol (III-[H,Me]-*S*) at the B3LYP/6-31G(d) Level of Theory

conformational assignment							
χ_2	χ_3	χ_{10}	χ_2	χ_3	χ_{10}	E (hartree)	rel E (kcal·mol⁻¹)
g^+	g^+	a	77.95	63.78	−176.82	−308.861 759 588	5.58
g^+	g^+	g^-	84.85	52.21	−39.81	−308.868 518 645	1.33
g^+	g^-	a	83.72	−74.52	175.99	−308.864 709 683	3.72
g^+	g^-	g^-	79.25	−71.11	−59.35	−308.864 078 627	4.12
a	g^+	a	−175.69	71.27	−171.49	−308.863 878 357	4.25
a	g^+	g^-	−174.20	56.59	−45.91	−308.870 644 238	0.00
a	a	g^+	−178.25	174.71	72.56	−308.866 380 432	2.68
a	a	a	179.74	174.65	177.60	−308.866 211 574	2.78
a	a	g^-	179.01	176.00	−66.05	−308.866 106 215	2.85
a	g^-	g^+	174.72	−58.47	48.62	−308.869 488 916	0.72
a	g^-	a	177.81	−72.18	174.53	−308.863 889 500	4.24
g^-	g^+	g^+	−79.71	68.49	66.38	−308.864 165 391	4.07
g^-	g^+	a	−83.12	73.27	−173.44	−308.864 450 066	3.89
g^-	a	g^+	−81.44	176.91	70.61	−308.864 404 100	3.92
g^-	a	a	−83.98	176.50	175.83	−308.864 066 200	4.13
g^-	a	g^-	−80.81	179.85	−63.76	−308.863 793 580	4.30

TABLE 11: Optimized Minima for the PEHS of (2R)-1-Methoxypropan-2-ol (III-[H,Me]-R) at the B3LYP/6-31G(d) Level of Theory

conformational assignment							
χ_2	χ_3	χ_{10}	χ_2	χ_3	χ_{10}	E (hartree)	rel E (kcal·mol^{-1})
g^+	a	g^+	80.81	−179.85	63.76	−308.863 793 580	4.30
g^+	a	a	83.98	−176.50	−175.83	−308.864 066 200	4.13
g^+	a	g^-	81.44	−176.91	−70.61	−308.864 404 100	3.92
g^+	g^-	a	83.12	−73.27	173.44	−308.864 450 067	3.89
g^+	g^-	g^-	79.71	−68.49	−66.38	−308.864 165 391	4.07
a	g^+	a	−177.81	72.18	−174.53	−308.863 889 500	4.24
a	g^+	g^-	−174.72	58.47	−48.62	−308.869 488 917	0.72
a	a	g^+	−179.01	−176.00	66.05	−308.866 106 219	2.85
a	a	a	−179.73	−174.65	−177.60	−308.866 211 567	2.78
a	a	g^-	178.26	−174.71	−72.56	−308.866 380 447	2.68
a	g^-	g^+	174.20	−56.59	45.91	−308.870 644 238	0.00
a	g^-	a	175.69	−71.27	171.50	−308.863 878 355	4.25
g^-	g^+	g^+	−79.25	71.11	59.35	−308.864 078 622	4.12
g^-	g^+	a	−83.72	74.52	−175.99	−308.864 709 683	3.72
g^-	g^-	g^+	−84.85	−52.21	39.81	−308.868 518 645	1.33
g^-	g^-	a	−77.95	−63.78	176.82	−308.861 759 588	5.58

by using the constructed PESs described above because they covered all the conformational space about the stereocenters.

$$\Delta E = \{[E_R(>\text{CHMe}) + E_S(>\text{CMeH})] - [E(>\text{CMe}_2) + E(>\text{CH}_2)]\} \quad (6)$$

According to Figure 5 and eq 6, the PESs of the four methyl-substituted analogues (cf. Figure 12) were added. The resulting values were used to produce another PES with ΔE energy values of about 0.0001 to 0.0007 hartree ($\sim$0.06−0.4 kcal·mol^{-1}). When the energy axis (z-axis) was calibrated to 1.0×10^{-3} hartree, which was the calibration used to produce the full PESs for analogues **IV-H$_2$**, **IV-Me$_2$**, **III-[H,Me]-S**, and **III-[H,Me]-R**, a resultant flat surface was produced (cf. Figure 14).

The same summation was performed on the four carbazole-substituted analogues from Figure 13, and the resulting values were plotted. The ΔE energy values produced from the summation were about 0.0005−0.009 hartree ($\sim$0.3−5.6 kcal·mol^{-1}), or about a factor of 10 larger than the PES produced for the methyl-substituted analogues. A flat surface was also produced when the calibration energy was reduced to 1.0×10^{-2} hartree (cf. Figure 15). (The raw data for Figures 12−15 are given in Supporting Information Tables S13 and S14.)

Given the above, the conformational energies of two prochiral structures can combine with the conformational energies of two enantiomers to produce a ΔE very close to zero. Although the ΔE energy values were not exactly zero, it would be expected that tight or very tight convergence threshold values would increase the number of zero significant digits for ΔE. With this is mind, it is of interest to ask the question, if the energetics of chiral compounds can be reproduced with achiral structures, would the administration of a mixture of two achiral structures have the same physiological effects as a racemic mixture of two enantiomers?

To the above question, the initial answer would seem to be no if one considers an asymmetrical molecular environment. In an asymmetrical environment, it is likely that only a chiral compound would have biological effects because nature would require a specific orientation for a biological effect. The latter statement is exemplified by the carvedilol β-adrenergic antagonist action; it is not expected that a mixture of two achiral compounds would have any β-adrenergic effects because only the S[-] configuration of carvedilol exerts action. This biological action would suggest an asymmetrical environment in which
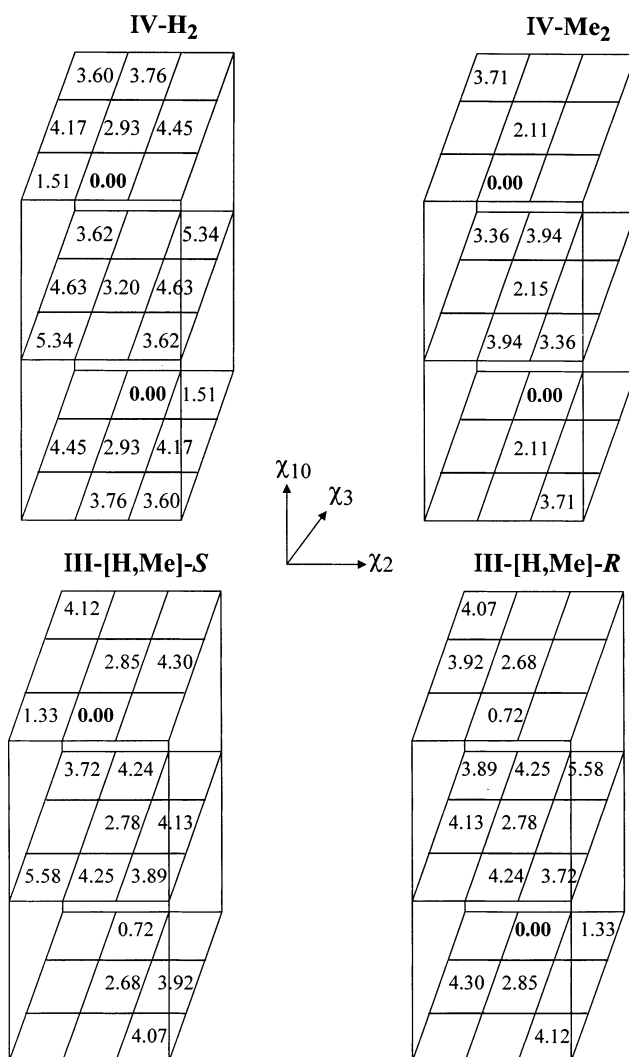

Figure 11. Graphical representation of the density functional computed PEHSs for **IV-H$_2$**, **IV-Me$_2$**, **III-[H,Me]-S**, and **III-[H,Me]-R** indicating all minima found and the associated relative energy in kcal·mol^{-1}. Minima that were not found have a blank space.

only a compound with a specific orientation (a chiral compound) could exert effects. However, if one considers symmetrical environments where enantiomers have equal activity, for
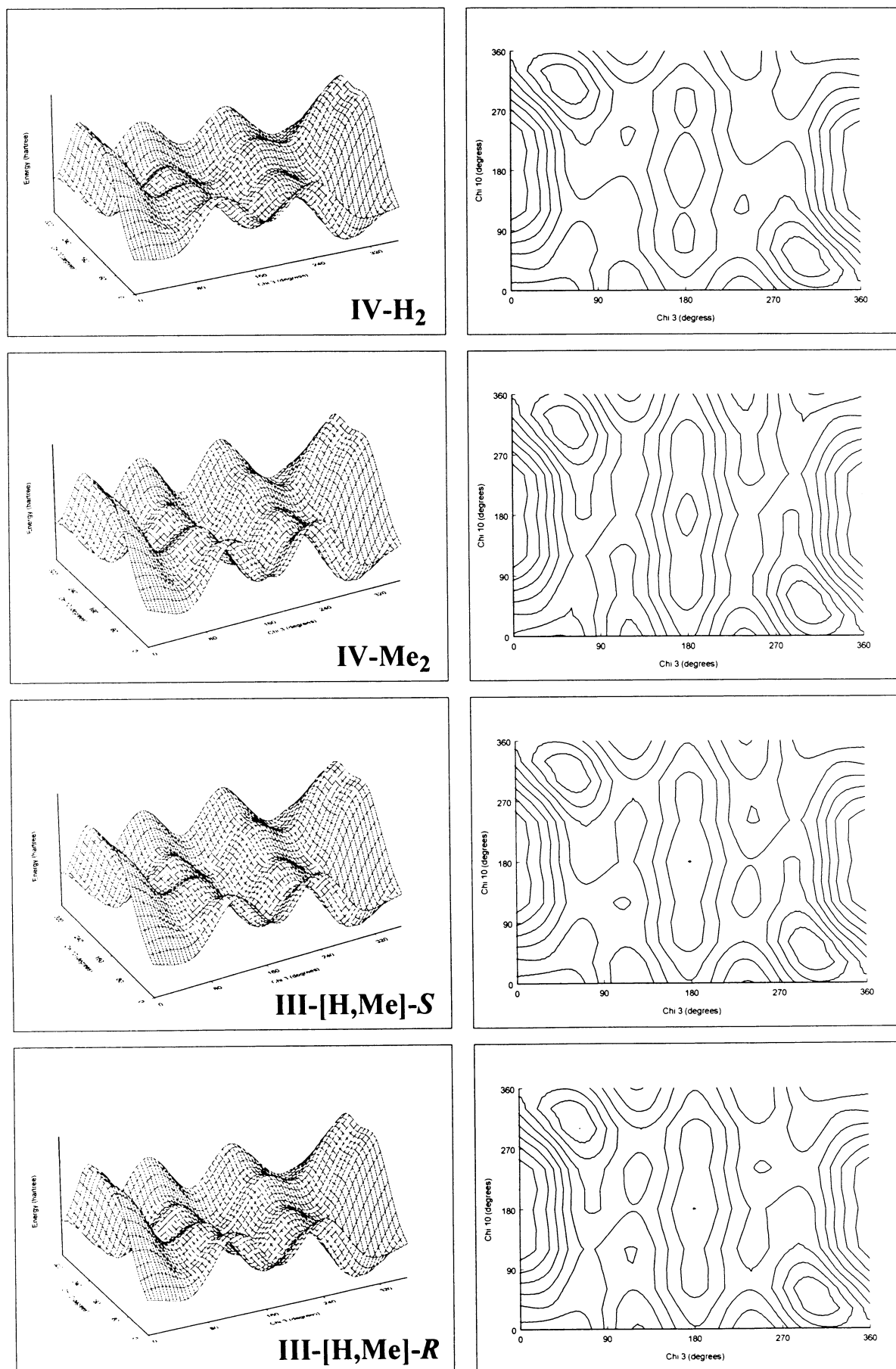
Enantiomeric Relationships of Carvedilol Fragment A

J. Phys. Chem. A, Vol. 107, No. 29, 2003 **5607**

Figure 12. PES [$E = f(\chi_3, \chi_{10})$] for (from top to bottom) 2-methoxyethan-1-ol (**IV-H$_2$**), 1-methoxy-2-methylpropan-2-ol (**IV-Me$_2$**), (2*S*)-1-methoxypropan-2-ol (**III-[H,Me]-*S***), and (2*R*)-1-methoxypropan-2-ol (**III-[H,Me]-*R***). The torsional angle χ_2 was frozen at 180.00° during the cross-sectional calculations of the PEHS.
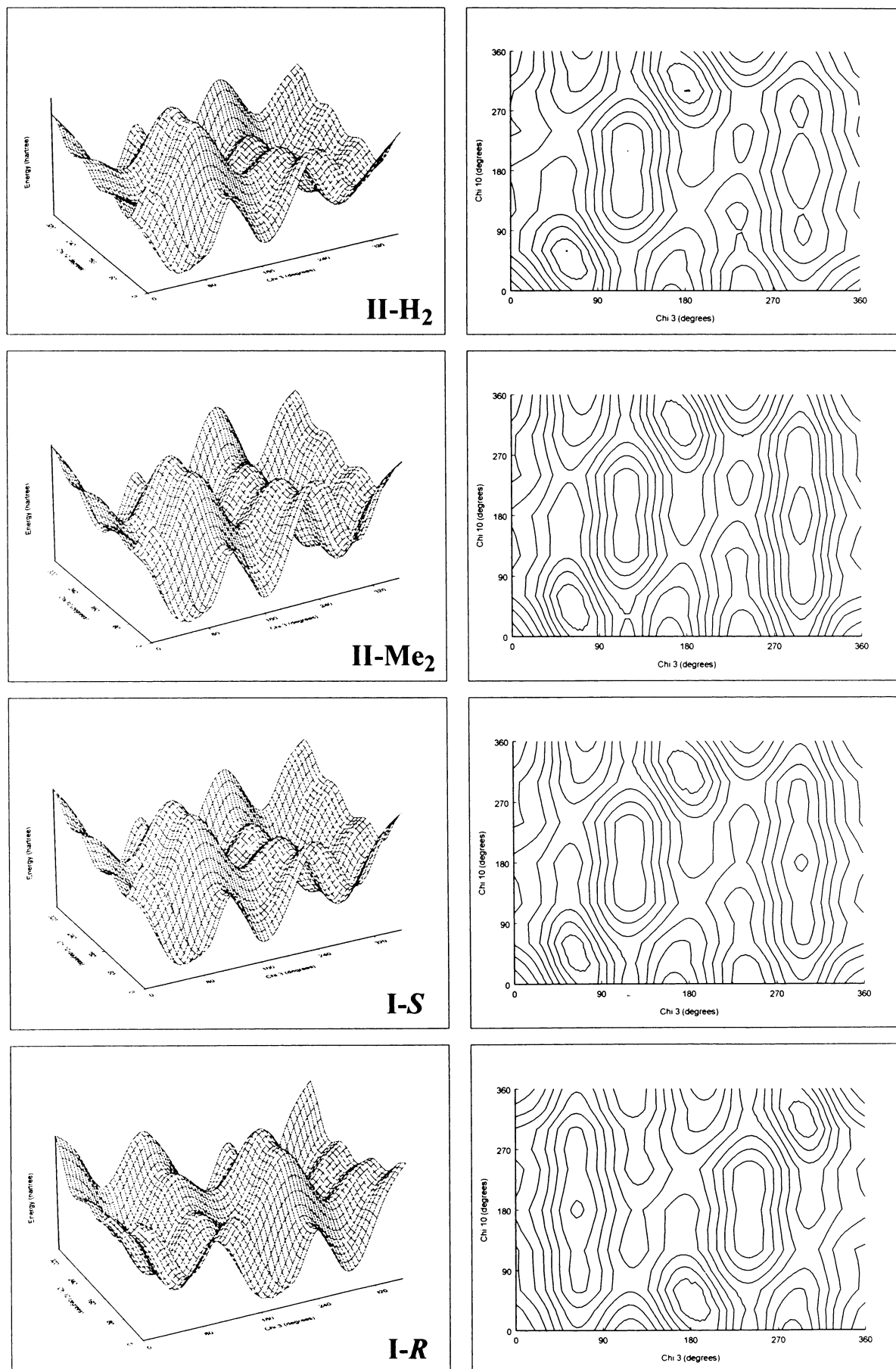
Figure 13. PES [$E = f(\chi_3,\chi_{10})$] for carbazole-containing analogues (from top to bottom): (2-hydroxyethoxy)carbazol (**II-H$_2$**), (2-hydroxy-2-methylethoxy)carbazol (**II-Me$_2$**), *S*-4-(2-hydroxypropoxy)carbazol (**I-S**), and *R*-4-(2-hydroxypropoxy)carbazol (**I-R**). The torsional angles χ_1 and χ_2 were frozen at 180.00° during the cross-sectional calculations of the PEHS.

Enantiomeric Relationships of Carvedilol Fragment A

J. Phys. Chem. A, Vol. 107, No. 29, 2003 **5609**
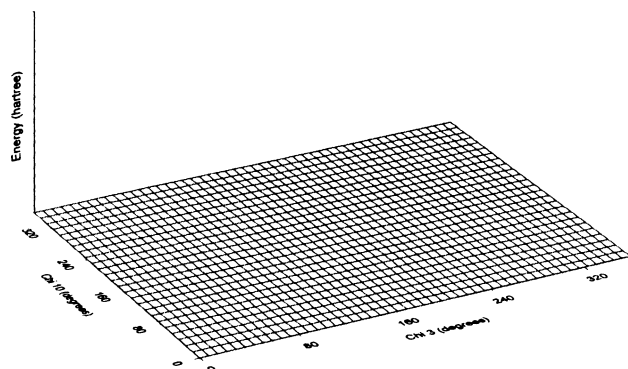
Figure 14. PES addition of carvedilol analogues (as illustrated in Figure 5) **IV-H$_2$**, **IV-Me$_2$**, **III-[H,Me]-*S***, and **III-[H,Me]-*R***.
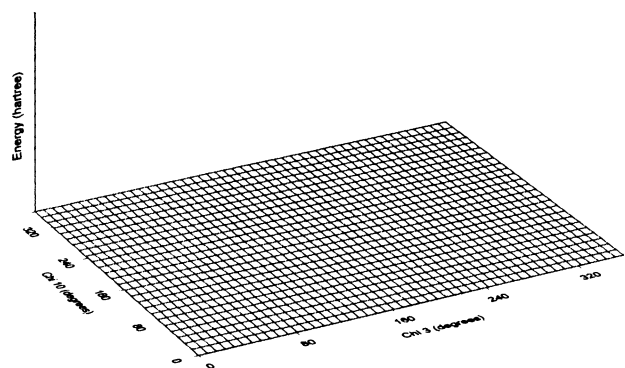
Figure 15. PES addition of carvedilol analogues (as illustrated in Figure 5) **II-H$_2$**, **II-Me$_2$**, **I-*S***, and **I-*R***.

example, carvedilol α_1-adrenergic antagonist and antioxidant effects, then would achiral compounds be able to produce qualitatively similar effects? Essentially, would a mixture of achiral carvedilol analogues similar to **II-H$_2$** and **II-Me$_2$** (at the stereocenter) be able to still produce α_1-adrenergic antagonist action and antioxidant activity, since it seems that these physiological effects can be produced without the need for chirality? Furthermore, at this stage one may wonder what would be the biological effects of administration of only one of the achiral structures.

Since the present work includes only gas phase results, more work is needed to shed light on these questions. Nonetheless, it would be tempting for drug design to be a fully achiral discipline so that, ideally, problems such as racemization at physiological pH, like that of thalidomide, could be circumvented. At the very least, however, the idea of equivalency between prochiral and chiral structures, as indicated by conformational energies, is a concept that must be clearly elucidated to see if any avenues could be exploited to aid processes like drug synthesis. Further, the data presented also demonstrate that the effects of chiral compounds are interdependent on the respective environment or medium they occupy because solely on the basis of molecular architecture, as quantified with conformational energies, some chiral properties can be both predicted and reproduced with achiral structures.

4. Conclusions

The carbazole-containing fragment of carvedilol, *R*- and *S*-4-(2-hydroxypropoxy)carbazol (fragment A), along with selected prochiral and chiral analogues, was subject to multidimensional conformational analysis (MDCA) of the full conformational

space at the ab initio and DFT levels of theory. Conformational analysis revealed the intrinsic energetic profiles associated with point chirality and axis chirality present in these structures. It is shown that axis chirality induced by an asymmetric distribution of electron density (generally as a result of asymmetric conformations) is a feature of all structures and, thus, does not require a point chiral center. Further, the combination of prochiral and chiral structures ($R-CH_2-OH$, [*R*] and [*S*] $R-CHMe-OH$, and $R-CMe_2-OH$) indicates that the conformational energetics of two enantiomers can be negated by the conformational energies of two achiral analogues. This illustrated the concept of energetic equivalency between achiral and chiral structures and may be an avenue that can be exploited in relevant fields such as drug design and synthesis.

Supporting Information Available: Tables of optimized minima for the PEHSs and of the summation values plotted in Figures 12−15. This material is available free of charge via the Internet at http://pubs.acs.org.

References and Notes

(1) Eriksson, T.; Björkman, S.; Roth, B.; Fyge, Å.; Höglund, P. Stereospecific determination, chiral inversion in vitro and pharmacokinetics in humans of the enantiomers of thalidomide. *Chirality* **1995**, *7*, 44−52.

(2) Strong, M. FDA Policy and Regulation of Stereoisomers: Paradigm Shift and the Future of Safer and More Effective Drugs. *Food Drug Law J.* **1999**, *54*, 463−488.

(3) Costante-Crassous, J.; Marrone, T. J.; Briggs, J. M.; McCammon, J. A.; Collet, A. Absolute Configuration of Bromochlorofluoromethane from Molecular Dynamics Simulation of Its Enantioselective Complexation by Cryptophane-C. *J. Am. Chem. Soc.* **1997**, *119* (16), 3818−3823.

(4) Carroll, F. A. *Perspectives on Structure and Mechanism in Organic Chemistry*; Brooks/Cole Publishing Company: Pacific Grove, CA, 1998; pp 78−80.

(5) Hirschmann, H.; Hanson, K. R. On factoring chirality and stereoisomerism. *Top. Stereochem.* **1983**, *14*, 183−229.

(6) Agosta, W. C. The Absolute Configuration of Pentadiendioic Acid. *J. Am. Chem. Soc.* **1964**, *86* (13), 2638−2642.

(7) Carlson, W.; Oberg, K. Clinical Pharmacology of Carvedilol. *J. Cardiovasc. Pharmacol. Ther.* **1999**, *4* (4), 205−218.

(8) Capomolla, S.; Febo, O.; Gnemmi, M.; Riccardi, G.; Opasich, C.; Carporotondi, A.; Mortara, A.; Pinna, G.; Cobelli, F. Beta-blockade therapy in chronic heart failure: diastolic function and mitral regurgitation improvement by carvedilol. *Am. Heart J.* **2000**, *139* (4), 596−608.

(9) Metra, M.; Nodari, S.; D'Aloia, A.; Bontempi, L.; Boldi, E.; Cas, L. D. A rationale for the use of beta-blockers as standard treatment for heart failure. *Am. Heart J.* **2000**, *139* (3), 511−521.

(10) Feuerstein, G.; Ruffolo, R. R., Jr. Beta-blockers in congestive heart failure: the pharmacology of carvedilol, a vasodilating beta-blocker and antioxidant, and its therapeutic utility in congestive heart failure. *Adv. Pharmacol. (San Diego)* **1998**, *42*, 611−615.

(11) Saijonmaa, O.; Metsarinne, K.; Fyhrquist, F. Carvedilol and its metabolites suppress endothelin-1 production in human endothelial cell culture. *Blood Pressure* **1997**, *6* (1), 24−28.

(12) Packer, M.; Bristow, M. R.; Cohn, J. N.; Colucci, W. S.; Fowler, M. B.; Gilbert, E. M.; Shusterman, N. H. The effect of carvedilol on morbidity and mortality in patients with chronic heart failure. U.S. Carvedilol Heart Failure Study Group. *N. Engl. J. Med.* **1996**, *334* (21), 1349−1355.

(13) Berg, M. A.; Chasse, G. A.; Deretey, E.; Fuzery, A. K.; Fung, B. M.; Fung, D. Y. K.; Henry-Riyad, H.; Lin, A. C.; Mak, M. L.; Mantas, A.; Patel, M.; Repyakh, I. V.; Staikova, M.; Salpietro, S. J.; Ting-Hua Tang; Vank, J. C.; Perczel, A.; Csonka, G. I.; Farkas, O.; Torday, L. L.; Szekely, Z.; Csizmadia, I. G. Prospects in computational molecular medicine: a millennial mega-project on peptide folding. *THEOCHEM* **2000**, *500*, 5−58.

(14) Feuerstein, G.; Yue, T. L.; Ma, X.; Ruffolo, R. R. Novel mechanisms in the treatment of heart failure: inhibition of oxygen radicals and apoptosis by carvedilol. *Prog. Cardiovasc. Dis.* **1998**, *41* (1 Suppl 1), 17−24.

(15) Searlee, A. J. F.; Gree, C.; Wilson, R. L. Ellipticines and carbazoles as antioxidants. In *Oxygen Radicals and Biology*; Borns, W., Saran, M., Tait, D., Eds.; Walter de Gruyter & Co.: Berlin, 1984; pp 377−381.

(16) Oldham, H. G.; Clarke, S. E. In vitro identification of the human cytochrome P450 enzymes involved in the metabolism of R(+)- and S(−)-carvedilol. *Drug Metab. Dispos.* **1997**, *25* (8), 970−977.

(17) Feuerstein, R.; Yue, T. L. A potent antioxidant, SB209995, inhibits oxygen-radical-mediated lipid peroxidation and cytotoxicity. *Pharmacology* **1994**, *48* (6), 385−391.

(18) Yue, T. L.; Mckenna, P. J.; Lysko, P. G.; Gu, J. L.; Lysko, K. A.; Ruffolo, R. R., Jr.; Feuerstein, G. Z. SB 211475, a metabolite of carvedilol, a novel antihypertensive agent, is a potent antioxidant. *Eur. J. Pharmacol.* **1994**, *251* (2−3), 237−243.

(19) Gehr, T. W.; Tenero, D. M.; Boyle, D. A.; Qian, Y.; Sica, D. A.; Shusterman, N. H. The pharmacokinetics of carvedilol and its metabolites after single and multiple dose oral administration in patients with hypertension and renal insufficiency. *Eur. J. Clin. Pharmacol.* **1999**, *55* (4), 269−277.

(20) van der Does, R.; Hauf-Zachariou, U.; Pfarr, E.; Holtbrugge, W.; Konig, S.; Griffiths, M.; Lahiri, A. Comparison of safety and efficacy of carvedilol and metoprolol in stable angina pectoris. *Am. J. Cardiol.* **1999**, *83* (5), 643−649.

(21) Ruffolo, R. R., Jr.; Gellai, M.; Hieble, J. P.; Willette, R. N.; Nichols, A. J. The pharmacology of carvedilol. *Eur. J. Clin. Pharmacol.* **1990**, *38* (Suppl 2), S82−S88.

(22) Oliveira, P. J.; Marques, M. P.; Batista de Carvalho, L. A. E.; Moreno, A. J. M. Effects of Carvedilol on Isolated Heart Mitochondria: Evidence for a Protonophoretic Mechanism. *Biochem. Biophys. Res. Commun.* **2000**, *276*, 82−87.

(23) Frisch, M. J.; Trucks, G. W.; Schlegel, H. B.; Scuseria, G. E.; Robb, M. A.; Cheeseman, J. R.; Zakrzewski, V. G.; Montgomery, J. A., Jr.; Stratmann, R. E.; Burant, J. C.; Dapprich, S.; Millam, J. M.; Daniels, A. D.; Kudin, K. N.; Strain, M. C.; Farkas, O.; Tomasi, J.; Barone, V.; Cossi, M.; Cammi, R.; Mennucci, B.; Pomelli, C.; Adamo, C.; Clifford, S.; Ochterski, J.; Petersson, G. A.; Ayala, P. Y.; Cui, Q.; Morokuma, K.; Malick, D. K.; Rabuck, A. D.; Raghavachari, K.; Foresman, J. B.; Cioslowski, J.; Ortiz, J. V.; Baboul, A. G.; Stefanov, B. B.; Liu, G.; Liashenko, A.; Piskorz, P.; Komaromi, I.; Gomperts, R.; Martin, R. L.; Fox, D. J.; Keith, T.; Al-Laham, M. A.; Peng, C. Y.; Nanayakkara, A.; Gonzalez, C.; Challacombe, M.; Gill, P. M. W.; Johnson, B. G.; Chen, W.; Wong, M. W.; Andres, J. L.; Head-Gordon, M.; Replogle, E. S.; Pople, J. A. *Gaussian 98* (Revision A.9); Gaussian, Inc.: Pittsburgh, PA, 1998.

(24) Becke, A. D. Density-functional thermochemistry. III. The role of exact exchange. *J. Chem. Phys.* **1993**, *98* (7), 5648−5652.

(25) *Axum 5.0C for Windows*; MathSoft Incorporated: 1996.

(26) Almeida, D. R. P.; Pisterzi, L. F.; Chass, G. A.; Torday, L. L.; Varro, A.; Papp, J. Gy.; Csizmadia, I. G. Density Functional Molecular Study on the Full Conformational Space of the *S*-4-(2-Hydroxypropoxy)-carbazol Fragment of Carvedilol (1-(9H-Carbazol-4-yloxy)-3-[2-(2-methoxyphenoxy)ethylamino]-2-propanol) in a Vacuum and in Different Solvent Media. *J. Phys. Chem. A* **2002**, *106* (43), 10423−10436.